Postnatal mechanical loading drives adaptation of tissues primarily through modulation of the non-collagenous matrix

D. E. Zamboulis[1], C. T. Thorpe[2], Y. Ashraf Kharaz[1], H. L. Birch[3], H. R. C. Screen[4], P. D. Clegg[1]

[1]Institute of Ageing and Chronic Disease, Faculty of Health and Life Sciences, University of Liverpool, Liverpool, L7 8TX, United Kingdom

[2]Comparative Biomedical Sciences, The Royal Veterinary College, Royal College Street, London, NW1 0TU, United Kingdom

[3]University College London, Department of Orthopaedics and Musculoskeletal Science, Stanmore Campus, Royal National Orthopaedic Hospital, Stanmore, HA7 4LP, United Kingdom

[4]Institute of Bioengineering, School of Engineering and Materials Science, Queen Mary University of London, London, E1 4NS, United Kingdom

Abstract

Mature connective tissues demonstrate highly specialised properties, remarkably adapted to meet their functional requirements. Tissue adaptation to environmental cues can occur throughout life and poor adaptation commonly results in injury. However, the temporal nature and drivers of functional adaptation remain undefined. Here, we explore functional adaptation and specialisation of mechanically loaded tissues using tendon; a simple aligned biological composite, in which the collagen (fascicle) and surrounding predominantly non-collagenous matrix (interfascicular matrix) can be interrogated independently. Using an

equine model of late development, we report the first phase-specific analysis of biomechanical, structural and compositional changes seen in functional adaptation, demonstrating adaptation occurs postnatally, following mechanical loading, and is almost exclusively localised to the non-collagenous interfascicular matrix. These novel data redefine adaptation in connective tissue, highlighting the fundamental importance of non-collagenous matrix and suggesting that regenerative medicine strategies should change focus from the fibrous to the non-collagenous matrix of tissue.

Introduction

Functional adaptation of load-bearing tissues such as tendon is crucial to ensure the tissue is specialised appropriately to meet functional needs. Adaptation to mechanical requirements is key in healthy development and homeostatic tissue maintenance, with poor tissue optimisation during maturation likely a key contributor to increased injury risk later in life. Dysregulated homeostasis and long-term under- or over-stimulation leads to maladaptation, changes in tissue integrity, and reduced mechanical competence and is implicated in the disease aetiology of load-bearing tissues (Freedman et al., 2015; Gardner et al., 2008). Understanding the developmental drivers of structural specialisation and their association with mechanobiology is thus of fundamental importance for healthy ageing and disease prevention in musculoskeletal tissues (Choi et al., 2018; Thorpe et al., 2013). Such knowledge will help identify future targets for therapeutic interventions, and thus address the current lack of effective musculoskeletal disease treatments with new, evidence-based approaches to disease management. However, there is currently little knowledge of the key extracellular matrix (ECM) components associated with structural specialisation, the temporal nature of their adaptation, or the stimuli that drive adaptation.

As the principal structural component of connective tissues, collagen expression at the gene

and protein level has been the focus of the majority of studies in relation to loading, with some studies reporting increases in collagen synthesis and others noting collagen degradation in response to loading, depending on the tissue function or tissue structure in different species (Choi et al., 2018; Magnusson & Kjaer, 2019). In tendons, this collagen structural framework is the fascicles and it is surrounded by the primarily non-collagenous and glycoprotein-rich components of the ECM, termed the interfascicular matrix (IFM) (Figure 1 – Figure supplement 1b) (Armiento et al., 2018; Thorpe & Screen, 2016). This distinction is important, as it describes a fibre composite material, in which "fascicle" and "IFM" phases have different mechanical properties, and overall tissue mechanical properties and function are governed by the interplay of these two phases. When looking to understand functional adaption of a tissue, it is necessary to look at adaption of all ECM components.

Whilst fascicle and collagen adaptation has received some attention, adaptation of the IFM phase to mechanical stimuli remains poorly defined. Indeed, it is notable that the numerous studies investigating the mechanoresponsive nature of load-bearing tissues tend to restrict their focus to specific fibre or matrix components with no spatial distinction, and also focus on a single element of either structural or mechanical adaptation, such that limited information is gained (Cherdchutham, Becker, et al., 2001; Choi et al., 2019; Mendias et al., 2012). In order to provide the necessary complete profile of adaptive behaviour, it is crucial that phase-specific, temporospatial adaptation in the context of both structure and function is defined.

Identifying the drivers of adaptation requires use of a model system in which the temporospatial nature of adaptation can be fully profiled. Tendon provides the ideal model for such a study. It is well-established that mature tendons can present structural and mechanical specialisms (Thorpe, Godinho, et al., 2015; Thorpe, Karunaseelan, et al., 2016; Thorpe, Riley, et al., 2016) and be grouped into two clear functional groups; stiff positional

tendons, such as the anterior tibialis tendon and the equine common digital extensor tendon (CDET), that simply connect muscle to bone to effectively position limbs, whilst elastic energy-storing tendons, such as the Achilles tendon and the equine superficial digital flexor tendon (SDFT), are further specialised to provide an energy storing function, increasing locomotor efficiency by stretching and storing energy which they return to the system on recoil (Alexander, 2002; Batson et al., 2003; Thorpe et al., 2012; Thorpe & Screen, 2016). Further, the simple aligned organisation of tendon means that fascicle and IFM phases are spatially distinct, enabling structural and mechanical characterisation of each phase independently (Thorpe et al., 2012; Thorpe & Screen, 2016). Finally, use of equine tendon provides access to an exceptional model of adaptation. The SDFT has been shown to be highly analogous to the human Achilles tendon in its capacity for energy storage, injury profile and extent of specialization and the anatomically opposing CDET is an example of a positional tendon, functionally comparable to the human anterior tibialis tendon (Figure 1 – Figure supplement 1a) (Biewener, 1998; Patterson-Kane & Rich, 2014). Availability of samples enabled us to explore the extensive adaptation processes associated with late stage development, contrasting paired positional and energy-storing equine tendons through pre- and post-natal development.

Using this model, we investigate the process and drivers of functional adaptation, when tendons transition from an absence of loading (foetal: mid to end (6 to 9 months) gestation, and 0 days: full-term foetuses, and foals that did not weight-bear); through to weight-bearing (0-1 month) and then to an increase in body weight and physical activity (3-6 months; and 1-2 years). We hypothesise that early in development during gestation, the fascicle and IFM of functionally distinct tendons have identical compositional profiles and mechanical properties, with tissue specialisation occurring as an adaptive response to the mechanical stimulus of load-bearing, predominantly in the IFM of the elastic energy-storing tendon.

Results

Mechanical adaptation is localised to the IFM

First, we determined how the mechanical properties of the fascicle and IFM develop in tendon, with a particular focus on the temporospatial nature of mechanical adaptation and functional specialisation. Individual fascicles were dissected while an isolated region of IFM was tested by shearing fascicles apart (Figure 1 – Figure supplement 1c). Samples were subjected to preconditioning followed by a pull to failure (Figure 1 – Figure supplement 1c). The yield point of samples was identified, denoting the point at which the sample became irreversibly damaged and was unable to recover from the applied load, and the sample failure properties also recorded, highlighting the maximum stress and strain the sample could withstand.

A significant increase in fascicle yield and failure properties was evident when comparing embryonic fascicles to those acquired immediately at birth (Figure 1h-i and 1e-g, respectively). However, data indicate minimal distinction in fascicle mechanics between functionally distinct tendons (Figure 1e-i) and, significantly, no specialisation for energy storage in response to loading during postnatal development.

Contrasting with fascicle mechanics, the failure properties of the IFM continued to alter throughout development with failure properties increasing markedly from 6 months onwards (Figure 2e-g). We also identify the emergence of an extended region of low stiffness at the start of the loading curve (ie an extended toe region) specific to the SDFT IFM pull to failure curve (Figure 2b). This indicates less resistance to extension, and together with the concomitant increase in IFM yield force and extension at yield (Figure 2h-i), demonstrates development of an overall greater capacity for extension in the SDFT IFM behaviour. A

summary of these findings is achieved by plotting the amount of IFM extension at different percentages of failure force (Figure 2j-k), highlighting how the IFM of the energy-storing SDFT became significantly less stiff than that of the positional CDET during the initial toe region of the loading curve as the tendon adapts.

The viscoelastic properties of the developing IFM also showed significant interactions between tendon type and development, with IFM viscoelasticity significantly decreasing with development specifically in the energy-storing SDFT (Figure 2a, c-d), resulting in specialisation towards a more energy efficient structure.

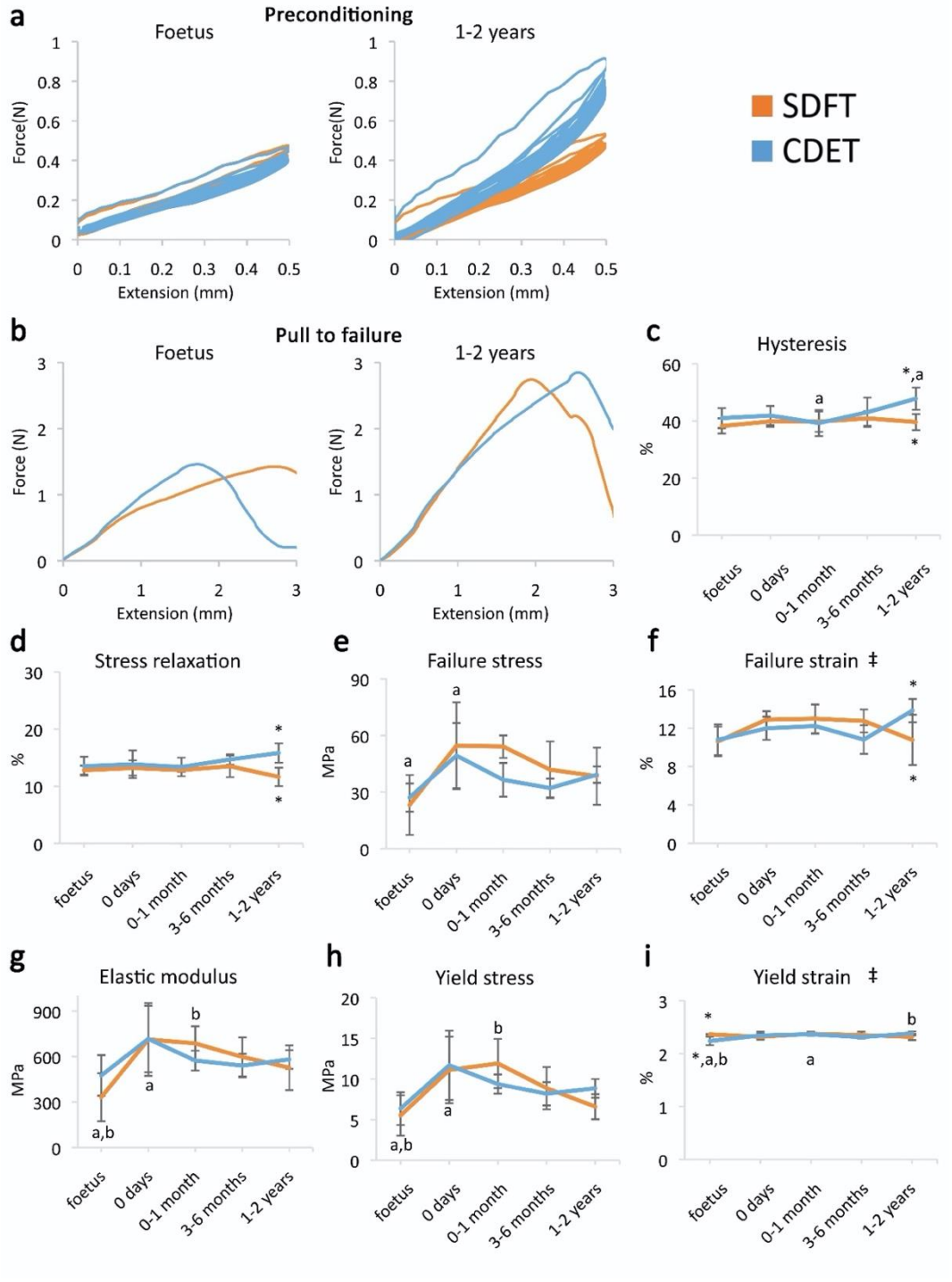

Figure 1. Fascicle response to mechanical testing shows increase in strength with development but few significant differences between tendon types, indicating that the fascicles show minimal structural specialisation in response to loading. (**a**) Representative curves for 10 preconditioning cycles for the SDFT and CDET fascicles in the foetus and 1-2 years age group. (**b**) Representative force-extension curves to failure for the SDFT and CDET fascicles in the same age groups. (**c-i**) Mean SDFT and CDET fascicle biomechanical properties are presented across development, with data grouped into age groups: foetus, 0 days (did not weight-bear), 0-1 month, 3-6 months, 1-2 years. ‡ significant interaction between tendon type and development, * significant difference between tendons, a-b significant difference between age groups. Error bars depict standard deviation. **Figure 1**

– **Figure supplement 1**. SDFT and CDET in the equine forelimb, tendon structure, and schematic showing procedure for biomechanical testing.

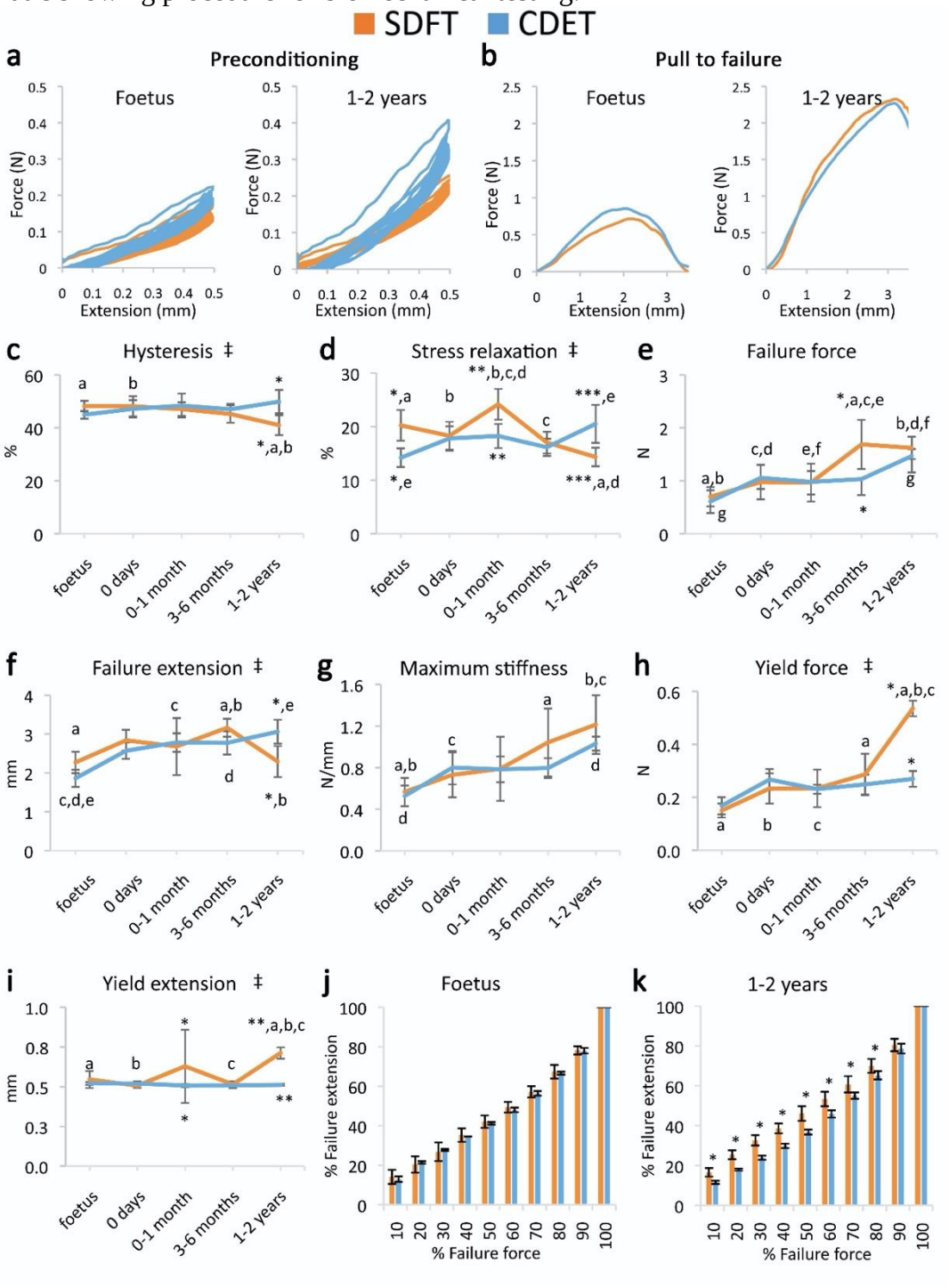

Figure 2. Mechanical testing of the IFM shows an equivalent increase in failure properties between the SDFT and CDET with development, but development of an extended low stiffness toe region and more elastic behaviour in the SDFT. (**a**) Representative curves for 10 preconditioning cycles for the SDFT and CDET IFM in the foetus and 1-2 years age group. (**b**) Representative force-extension curves to failure for the SDFT and CDET IFM in the same age groups. (**c-i**) Mean SDFT and CDET IFM biomechanical properties are presented across development, with data grouped into age groups: foetus, 0 days (did not weight-bear), 0-1 month, 3-6 months, 1-2 years. (**j-k**) To visualise the extended low stiffness toe region in the SDFT IFM, the amount of IFM

extension at increasing percentages of failure force is presented, comparing the SDFT and CDET in the foetus and 1-2 years age group. ‡ significant interaction between tendon type and development, * significant difference between tendons, a-g significant difference between age groups. Error bars depict standard deviation.

Structural adaptation is localised to the IFM

Having described the mechanical adaptation of the IFM to meet functional demand, we next performed a histological and immunohistochemical comparison of developing energy-storing and positional tendons to determine how temporospatial structural adaptation may dictate this evolving mechanical behaviour.

The energy-storing SDFT and positional CDET appeared histologically similar in the foetus, in both instances showing surprisingly poor demarcation of the IFM, which only became structurally distinct after birth and the initiation of loading (Figure 3a). Fascicle development was generally consistent in both tendon types with cellularity and crimp showing a reduction with development, cells displaying more elongated nuclei, and collagen showing a more linear organisation (Figure 3b, Figure 3 – Figure supplement 1, scoring criteria Supplementary File 1). In contrast, the IFM demonstrated divergence between tendon types with only the SDFT IFM showing an increase in cellularity following tendon loading and a retention of IFM width throughout development (Figure 3b, Figure 3 – Figure supplement 1).

The abundance of major ECM proteins was also generally consistent across fascicle and IFM in the foetus, with divergence of protein composition between phases only evident with further development (Figure 4). Notably adaptation was driven by changes in non-collagenous ECM components specifically, levels of which reduced in the fascicles and increased dramatically in the IFM through postnatal development (Figure 4, Figure 4 – Figure supplement 1). Of particular note, we demonstrate PRG4 (commonly known as lubricin) and TNC were predominantly found in the IFM of tendons and showed sparse staining or were absent, respectively, from the fascicles. We also demonstrate that elastin is preferentially

localised to the IFM with its abundance decreasing only in the CDET with development. Furthermore, we show histological and compositional changes manifest after birth and with the initiation of loading, but that histological and compositional adaptation to loading then occurs over a period of months, involving both upregulation and downregulation of different histologic variables and ECM constituents.

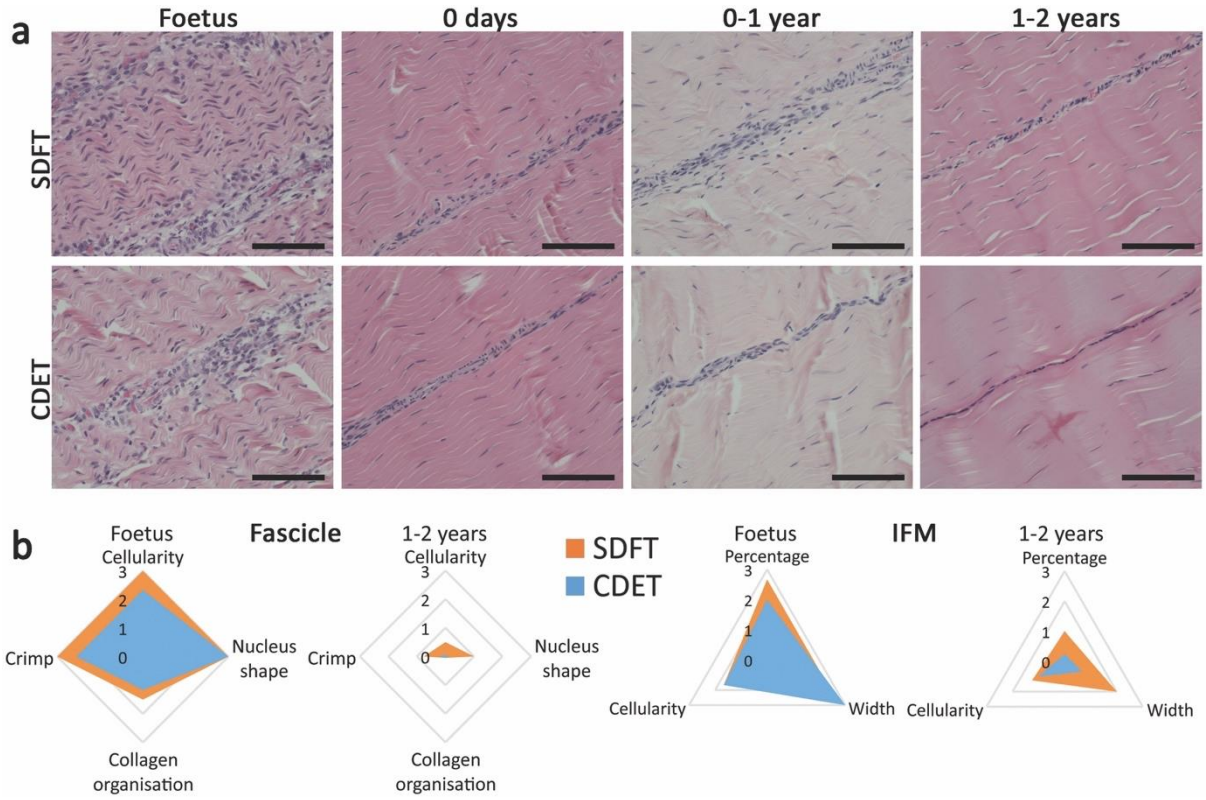

Figure 3. The SDFT and CDET are histologically similar at birth and differentiate with development especially in the IFM. (**a**) Representative images of H&E sections of the SDFT and CDET demonstrate structural development: foetus, 0 days (did not weight-bear), 0-1 year, and 1-2 years whilst (**b**) Radar plots enable the mean histology scores of the fascicle and IFM for the SDFT and CDET to be compared between the foetus and 1-2 years age group (all data shown in Figure 3 – Figure supplement 1 and scoring criteria in Supplementary File 1). A decrease in cell numbers, crimp, and IFM width is visible with progression of age, and the aspect ratio of cells in the fascicle increases. Scale bar 100 μm.
Figure 3 – Figure supplement 1. Scoring of histologic variables for the IFM and fascicle in the SDFT and CDET through postnatal development.

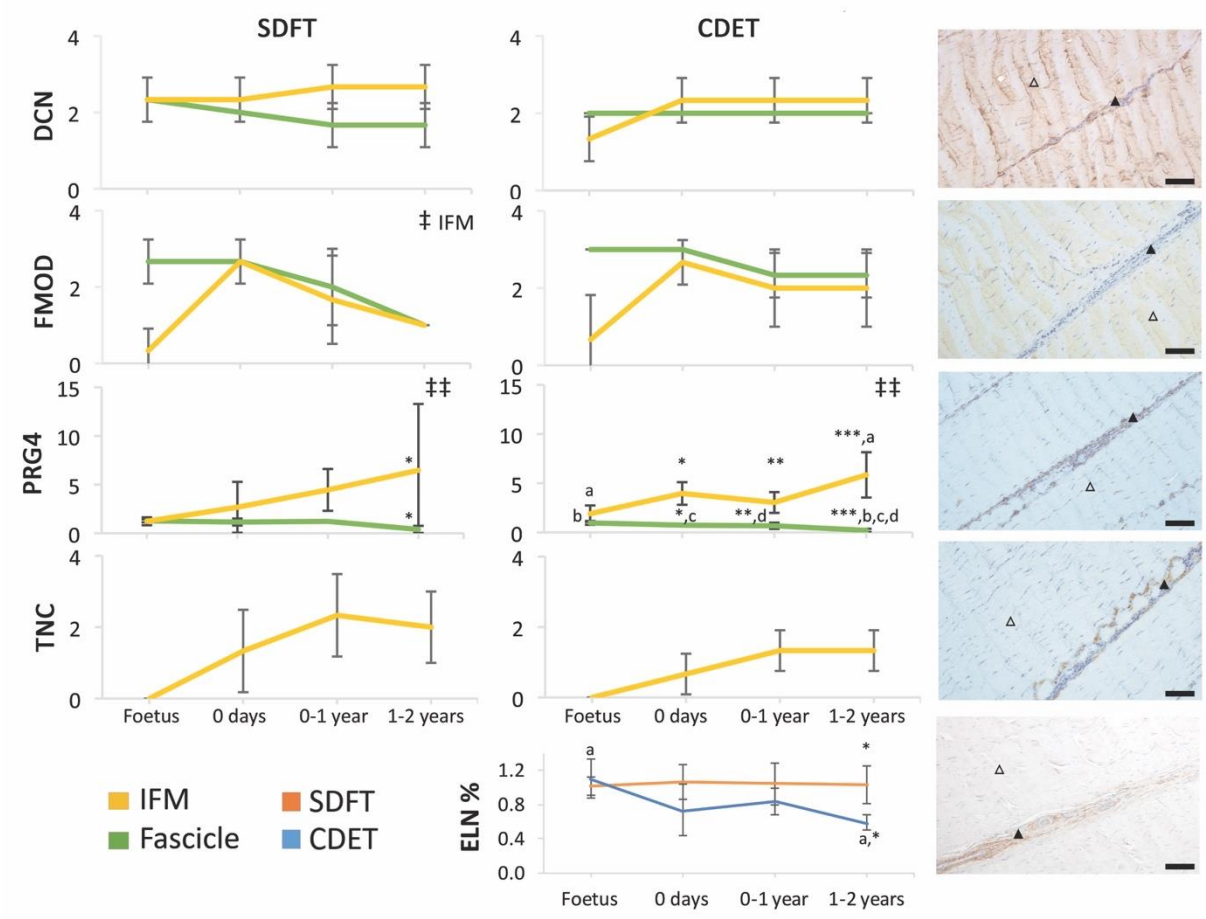

Figure 4. Immunohistochemical assays show divergence of PGR4 (lubricin) and elastin with maturation between functionally distinct tendons. IFM and fascicle staining scores are shown for decorin (DCN), fibromodulin (FMOD), lubricin (PRG4), and tenascin-C (TNC) in the SDFT and CDET, alongside representative images of immunohistochemical staining in the postnatal SDFT. DCN and FMOD staining is found in both IFM (black triangle) and fascicle (white triangle). PRG4 staining in mainly located in the IFM (black triangle) and less staining can be found in the fascicle (white triangle). TNC staining is restricted to the IFM (black triangle) and absent from the fascicle (white triangle). A quantitative measure of elastin (ELN) is provided as percentage of wet weight, alongside a representative image of immunohistochemical staining in the postnatal SDFT. ELN staining is mainly located in the IFM (black triangle) and faint staining can be found in the fascicle (white triangle). Staining scores for elastin are provided in Figure 4 – Figure supplement 1. ‡ significant change in tendon phase with development, ‡‡ significant interaction between tendon phase and development, * significant difference between tendons, a-d significant difference between age groups. Scale bar 100 μm. Error bars depict standard deviation.
Figure 4 – Figure supplement 1. Scoring of ELN staining for the IFM and fascicle in the SDFT and CDET through postnatal development.

Adaptation relies on evolution of IFM composition only

To explore these concepts in further detail and to scrutinise the capacity for ECM adaptation, proteomic methodologies were adopted. With the mechanical and histological data identifying that functional adaptation is particular to the energy-storing SDFT, mass spectrometry analysis focused on a more detailed comparison of the IFM and fascicle development and adaptation in this tendon specifically.

Our results demonstrated that the proteomic profile of the IFM was more complex (more identified proteins) and a higher percentage of IFM proteins were cellular (Figure 5 – Figure supplement 1), supporting the histological findings of a more cellular IFM. Notably, despite the two phases being structurally distinct, they had 14 collagens and 11 proteoglycans in common (Supplementary File 4). Overall, proteomic heatmap analysis correlated very strongly with immunohistochemical findings, showing that alterations in the fascicle proteome reduced through development, with minimal changes following the initiation of loading (Table 1 and 2, Figure 5a), whilst numerous matrisome and matrisome-related proteins progressively increase in abundance through development in the IFM (Table 1 and 2, Figure 5a). Detailed consideration of protein changes also highlights that post loading changes in the IFM appear more specific to proteoglycans and glycoproteins. Correlation analysis of IFM matrisome protein abundance and mechanical properties of the IFM across development revealed correlations for matrisome proteins abundance with the mechanical properties correlating IFM ECM composition and functional adaptation. Significant correlations included a negative correlation between proteoglycans DCN, LUM, OGN, PRELP and COL3A1 and the IFM hysteresis, a positive correlation between FBLN5 and stress relaxation, a positive correlation between COL6A1, COL6A2, and OGN and maximum stiffness, and for the yield properties a positive correlation of proteoglycans DCN, LUM, OGN, PRELP and COL3A1 and force at yield point (Supplementary File 5). In addition,

protein abundance for BGN, DCN, COMP, COL1A2, COL3A1 in the IFM and COMP and COL3A1 in the fascicles across development is mirrored by whole tendon mRNA expression (Figure 5 – Figure supplement 2).

Proteomic data also enabled insight into the turnover of proteins in the different tendon phases, through a comparison of the neopeptides produced by protein breakdown (Thorpe, Peffers, et al., 2016). In the current study, we were able to profile the temporal nature of fascicle and IFM turnover, demonstrating that both phases display turnover during development but that fascicle turnover slows down towards the end of maturation, whilst IFM turnover rates are maintained, suggesting structural and/or compositional plasticity (Figure 5b).

Having identified the IFM as the location of functional adaptation, we next investigated the regulation of this process, to detect targets for modulation for regeneration strategies addressing functional impairment. For this purpose, pathway analysis was carried out for the differentially abundant proteins identified with mass spectrometry across age groups using the Ingenuity Pathway Analysis software (IPA). Pathway analysis revealed the canonical pathways “integrin signaling” and “actin cytoskeleton signaling” were predicted to be activated with development in the IFM supporting an ECM-integrin-cytoskeleton to nucleus signalling pathway for the mediation of the observed mitogenesis and matrigenesis in response to tendon loading. In addition, pathway analysis identified TGFB1 as an upstream regulator for the IFM dataset and based on the IFM protein abundance across age groups predicted TGFB1 to be inhibited in the foetus age group and to become activated in the 3-6 months age group. TGF-β1 was therefore highlighted as a potential regulator of ECM organisation and functional adaptation, predicted to be upregulated in the energy-storing tendon following loading (Figure 6a). This was supported by TGB1 mRNA expression in whole tendon increasing in the 3-6 months SDFT only, with the positional CDET TGFB1

expression showing no change with development (Figure 6b). In addition, knockdown of TGFB1 in equine adult tenocytes and stimulation with 10 ng recombinant TGF-β1 showed downregulation and upregulation, respectively, of key ECM components, BGN, COMP, COL1A2, and COL3A1, supporting a regulatory role for TGF-β1 (Figure 6c-d). Finally, correlation analysis of TGFB1 mRNA expression of whole tendon and IFM matrisome protein abundance across development revealed positive correlations with ECM proteins which were significant for COL1A2, COL2A1, COL4A1, COL4A2, COL6A3, HSPG2, and FN1 (Supplementary File 6).

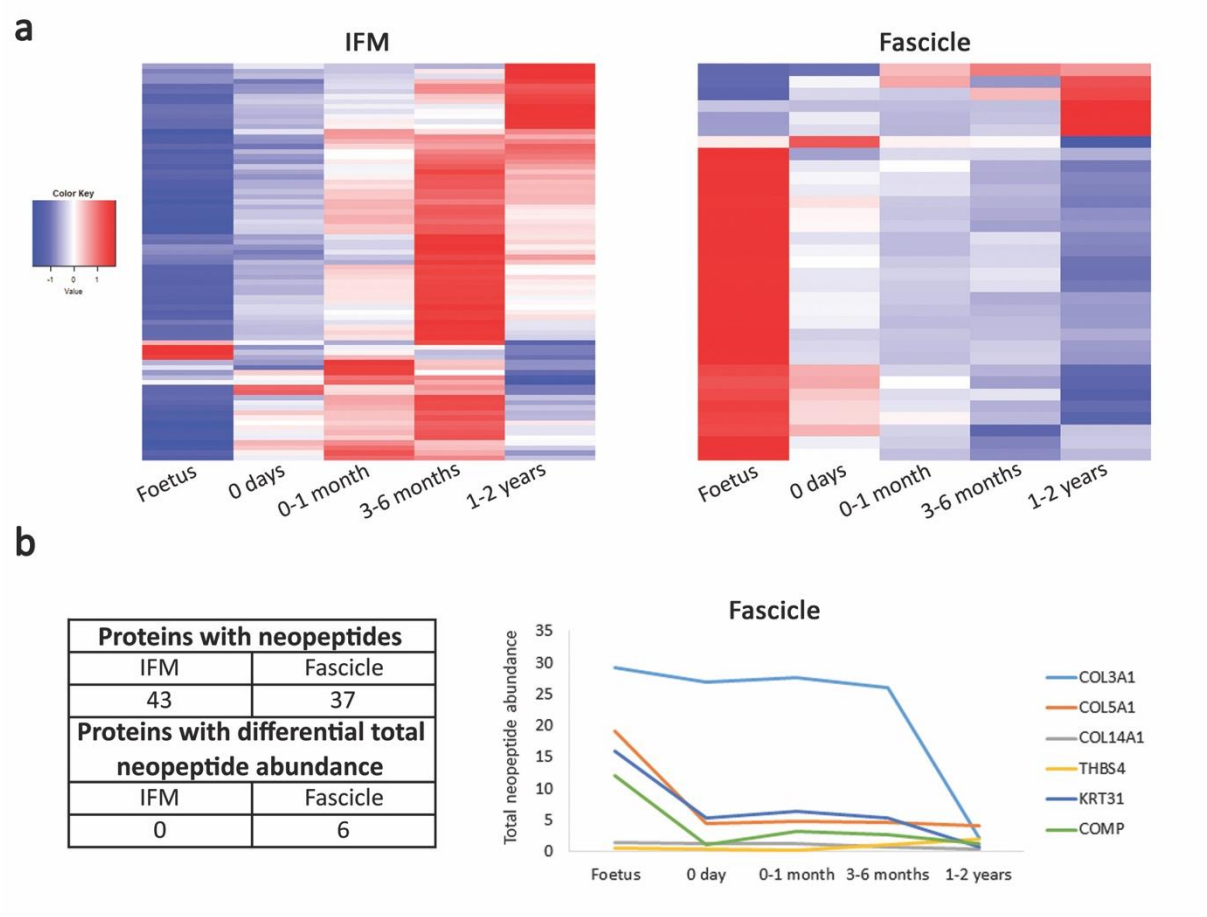

Proteins with neopeptides	
IFM	Fascicle
43	37
Proteins with differential total neopeptide abundance	
IFM	Fascicle
0	6

Figure 5. The fascicle proteome remains the same during postnatal development and tendon loading whereas the IFM proteome starts changing following tendon loading in postnatal development. (**a**) Heatmap of differentially abundant proteins in foetus, 0 days (did not weight-bear), 0-1 month, 3-6 months, and 1-2 years SDFT IFM and fascicles (p<0.05, fold change ≥2). Heatmap colour scale ranges from blue to white to red with blue representing lower abundance and red higher abundance. (**b**) Proteins with identified neopeptides and proteins showing differential total neopeptide abundance across age groups. Graph of proteins showing differential total neopeptide abundance in the SDFT fascicles across development (p<0.05, fold change≥2, FDR 5%). No proteins showed differential total neopeptide abundance in the IFM. **Figure 5 – Figure supplement 1**. Classification of SDFT IFM and fascicle identified proteins and differentially abundant proteins according to their associated location. **Figure 5 – Figure supplement 2**. Relative mRNA expression of major ECM genes in whole tissue SDFT and CDET through postnatal development.

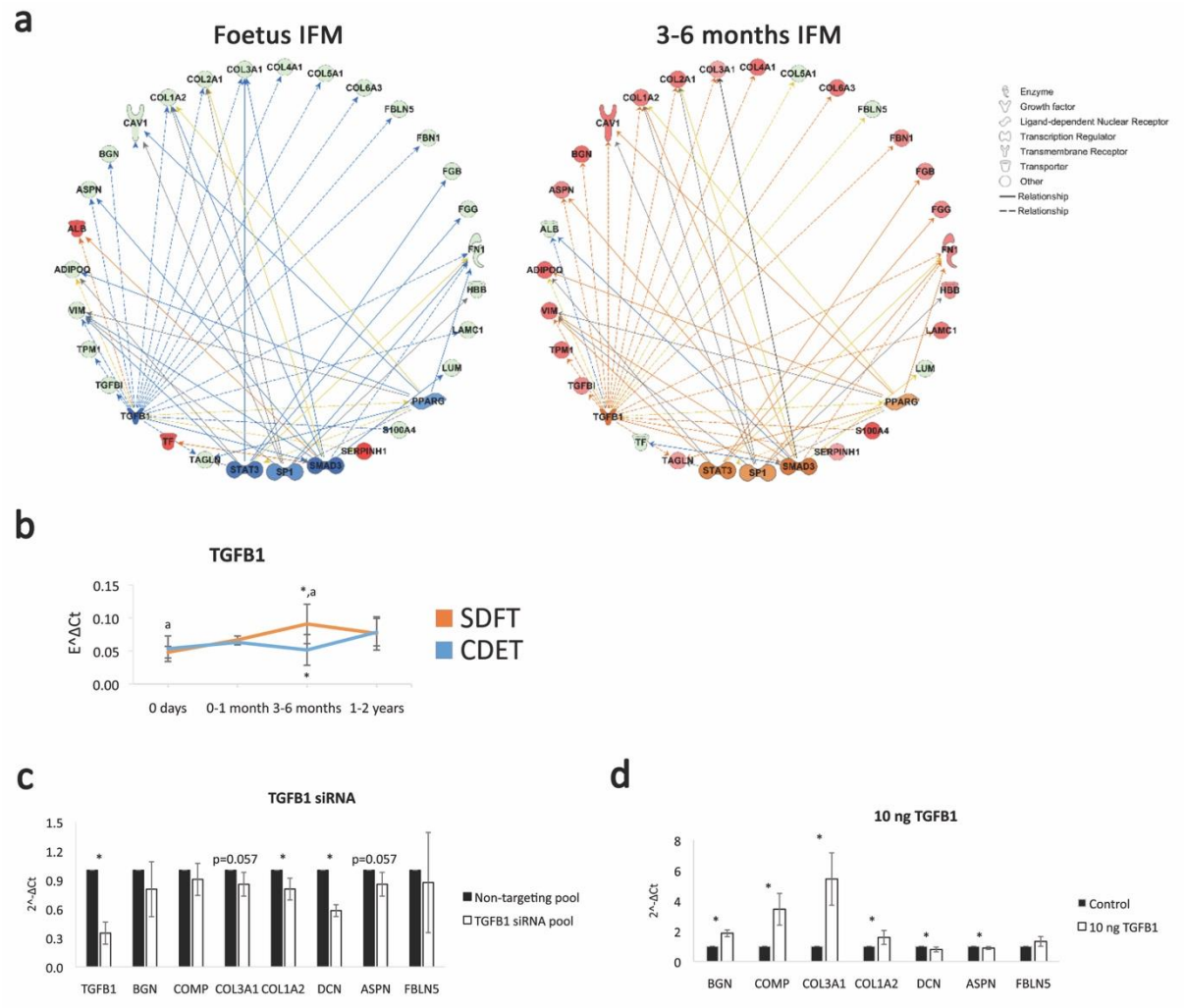

Figure 6. TGFB1 is predicted to be involved in compositional changes observed in the IFM. (**a**) IPA networks for TGFB1 as an upstream regulator were generated for the foetus and 3-6 months SDFT IFM proteomic datasets. TGFB1 regulation in the IFM is predicted to be inhibited in the foetus and activated at 3-6 months in the SDFT. Red nodes, upregulated proteins, green nodes, downregulated proteins, intensity of colour is related to higher fold-change, orange nodes, predicted upregulated proteins in the dataset, blue nodes, predicted downregulated proteins. (**b**) Whole tendon relative mRNA expression for TGFB1 in the SDFT and CDET during postnatal development shows an increase in TGFB1 mRNA in the 3-6 months highly-loaded SDFT only. * significant difference between tendons, a significant difference between age groups. (**c-d**) Relative mRNA expression of major ECM genes predicted to be regulated by TGFB1 in the IPA network following TGB1 knockdown (c) and stimulation with 10 ng recombinant TGF-β1 (d) for 24 hours. BGN, DCN, COMP, COL1A2 and COL3A1 show regulation following TGFB1 knockdown or addition. * significant difference between control and treatment. Error bars depict standard deviation.

Table 1. IFM differentially abundant matrisome and matrisome-associated proteins through development organised by highest mean condition ($p<0.05$, fold change≥2). Proteins are arranged into colour coded divisions and categories. Bar graphs profile the relative abundance of each protein at each development stage, a foetus, b 0 days, c 0-1 month, d 3-6 months, e 1-2 years, with the development age reporting the highest mean protein level also specified.

Protein	Division	Category	Highest mean cond.	a b c d e
SERPINH1	Matrisome-associated	ECM Regulators	Foetus	
COL14A1	Core matrisome	Collagens	0-1 month	
ASPN	Core matrisome	Proteoglycans	0-1 month	
FMOD	Core matrisome	Proteoglycans	0-1 month	
KERA	Core matrisome	Proteoglycans	0-1 month	
FBLN5	Core matrisome	ECM Glycoproteins	0-1 month	
FGB	Core matrisome	ECM Glycoproteins	0-1 month	
FGG	Core matrisome	ECM Glycoproteins	0-1 month	
COL1A2	Core matrisome	Collagens	3-6 months	
COL2A1	Core matrisome	Collagens	3-6 months	
COL4A1	Core matrisome	Collagens	3-6 months	
COL4A2	Core matrisome	Collagens	3-6 months	
COL6A3	Core matrisome	Collagens	3-6 months	
BGN	Core matrisome	Proteoglycans	3-6 months	
HSPG2	Core matrisome	Proteoglycans	3-6 months	
ADIPOQ	Core matrisome	ECM Glycoproteins	3-6 months	
FBN1	Core matrisome	ECM Glycoproteins	3-6 months	
FN1	Core matrisome	ECM Glycoproteins	3-6 months	
LAMB2	Core matrisome	ECM Glycoproteins	3-6 months	
LAMC1	Core matrisome	ECM Glycoproteins	3-6 months	
NID1	Core matrisome	ECM Glycoproteins	3-6 months	
ANXA4	Matrisome-associated	ECM-affiliated	3-6 months	
S100A4	Matrisome-associated	Secreted Factors	3-6 months	
COL21A1	Core matrisome	Collagens	1-2 years	
COL3A1	Core matrisome	Collagens	1-2 years	
COL5A1	Core matrisome	Collagens	1-2 years	
COL5A2	Core matrisome	Collagens	1-2 years	
COL6A1	Core matrisome	Collagens	1-2 years	
COL6A2	Core matrisome	Collagens	1-2 years	
DCN	Core matrisome	Proteoglycans	1-2 years	
LUM	Core matrisome	Proteoglycans	1-2 years	
OGN	Core matrisome	Proteoglycans	1-2 years	
PRELP	Core matrisome	Proteoglycans	1-2 years	
COMP	Core matrisome	ECM Glycoproteins	1-2 years	
DPT	Core matrisome	ECM Glycoproteins	1-2 years	

TGFBI	Core matrisome	ECM Glycoproteins	1-2 years	

Table 2. Fascicle differentially abundant matrisome and matrisome-associated proteins through development organised by highest mean condition (p<0.05, fold change≥2). Proteins are arranged into colour coded divisions and categories. Bar graphs on the right profile the relative abundance of each protein at each development stage, a foetus, b 0 days, c 0-1 month, d 3-6 months, e 1-2 years, with the development age reporting the highest mean protein level also specified.

Protein	Division	Category	Highest mean cond.	a b c d e
COL11A1	Core matrisome	Collagens	Foetus	
DCN	Core matrisome	Proteoglycans	Foetus	
FMOD	Core matrisome	Proteoglycans	Foetus	
KERA	Core matrisome	Proteoglycans	Foetus	
PCOLCE	Core matrisome	ECM Glycoproteins	Foetus	
SERPINF1	Matrisome-associated	ECM Regulators	Foetus	
ANXA1	Matrisome-associated	ECM-affiliated Proteins	Foetus	
ANXA2	Matrisome-associated	ECM-affiliated Proteins	Foetus	
ANXA5	Matrisome-associated	ECM-affiliated Proteins	Foetus	
LGALS1	Matrisome-associated	ECM-affiliated Proteins	Foetus	
COL12A1	Core matrisome	Collagens	0 days	
COL3A1	Core matrisome	Collagens	1-2 years	
PRELP	Core matrisome	Proteoglycans	1-2 years	
COMP	Core matrisome	ECM Glycoproteins	1-2 years	
FN1	Core matrisome	ECM Glycoproteins	1-2 years	

Discussion

In this study, we describe the phase-specific process and drivers of functional adaptation in tendon development integrating mechanical, structural, and compositional analysis in tendons transitioning from an absence of loading through to weight-bearing and then to an increase in body weight and physical activity. To investigate functional adaptation and structure-function specialisation, we are contrasting fascicles and IFM of two tendons with distinct functions and mechanical properties; the equine SDFT and CDET. The energy-storing SDFT, which

functions by stretching and recoiling with each stride to store and return energy, undergoes peaks strains recorded at 16.6 % *in vivo* and has been found to be significantly more extensible than the CDET. The positional CDET, which functions to extend the distal limb prior to limb placement and is relatively inextensible to allow precise placement of the limb, experiences much lower strains than the SDFT (estimated at 2.5 %) and is less extensible than the SDFT (Batson et al., 2003; Birch et al., 2008; Thorpe et al., 2012).

Whilst the limited previously available data on the development of tendon gross mechanical properties show an increase in mechanical properties with development (Ansorge et al., 2011; Cherdchutham, Meershoek, et al., 2001), no such phase-specific analysis of the development of tissue mechanics has been carried out previously. Similarly, available research into tendon morphogenesis and maturation has previously focused on the development of the collagenous network that comprises the tendon fascicles and is often focussed on early foetal development (Kalson et al., 2011; Marturano et al., 2013; Pan et al., 2018). Murine and zebrafish models used to investigate tendon development and adaptation have advanced our understanding of the control of fibrillogenesis by ECM proteins (Subramanian et al., 2018; Subramanian & Schilling, 2014; Taye et al., 2020) but these models lack an IFM, thus restricting our ability to explore the functional specialism we see in humans and other larger mammals.

Here, examining the fascicle and IFM mechanical properties independently, we show minimal distinction in fascicle mechanics between functionally distinct tendons and, significantly, no specialisation for energy storage in response to loading during postnatal development. In contrast, the IFM mechanical properties display continuous alterations through development with the properties of the IFM in the foetus being comparable between functionally distinct tendons, and a low stiffness region emerging in the initial non-linear region (toe region) of the pull to failure curve of the SDFT IFM only following tendon loading postnatally. This is coupled with a concomitant increase in IFM force and extension

362 at yield, the point at which the sample became irreversibly damaged, highlighting that the
363 energy-storing SDFT IFM becomes significantly less stiff than that of the positional CDET
364 during the initial toe region of the loading curve. We have previously indicated that this low
365 stiffness behaviour allows sliding between the fascicles, enabling non-uniform loading of
366 tissue and is fundamental for effective extension and recoil in energy-storing tendons
367 (Thorpe, Godinho, et al., 2015). Furthermore, with ageing the low stiffness behaviour of the
368 energy-storing IFM is lost, possibly contributing to disease development (Thorpe et al.,
369 2013). The only other studies considering the mechanical properties of developing tendons
370 have focused simply on changes in whole tissue mechanics, and have thus not been able to
371 identify the drivers of change within the tissue (Ansorge et al., 2011; Cherdchutham,
372 Meershoek, et al., 2001). Here, we identify that the IFM is the key region in which
373 mechanical adaptation to meet function occurs, and that this occurs after the initiation of
374 loading, primarily 1-2 years postnatally.

375 We subsequently examine how temporospatial structural adaptation may dictate this evolving
376 mechanical behaviour and uncover a divergence in structural characteristics between tendon
377 types in the IFM only, with a retention of IFM width throughout development and an increase
378 in cellularity in the SDFT IFM only. It is well recognised that foetal and early postnatal
379 tendons are highly cellular, and cellularity is generally considered to decrease postnatally
380 (Russo et al., 2015; Stanley et al., 2008), but here we show that the described reduction in
381 cellularity only occurs in the fascicles, and cellularity in fact increases in the IFM with
382 development. By following the alterations in cellularity across IFM and fascicle, here we can
383 determine that the marked difference in regional cellularity is likely driven by a maintenance
384 of cell numbers following tendon loading in the thinning IFM, while cell numbers in the
385 fascicle appear to reduce as a result of the fascicle ECM increase. Greater cellularity is
386 commonly associated with a requirement for rapid adaptive organisation of ECM components

(Russo et al., 2015), suggesting the IFM, particularly in the energy-storing tendons, may adapt to be more mechanoresponsive, a necessary aspect of healthy homeostatic maintenance of a tissue. Immunohistochemical analysis reveals the distribution of major ECM proteins is consistent across tendons in the foetus and becomes distinct across compartments through development. Of note, PRG4 (lubricin), a large proteoglycan which is important in ECM lubrication, is found mainly distributed in the IFM of tendons. Using a lubricin-knockout mouse, this proteoglycan has been demonstrated to facilitate interfascicular sliding (Kohrs et al., 2011), indicating that this structural adaptation may be key in achieving the previously identified mechanical adaptation in the energy-storing tendon IFM. In addition, Kostrominova and Brooks (2013) (Kostrominova & Brooks, 2013) report PRG4 expression as wells as elastin expression decreased with ageing in rat tendon suggesting an association with an increased risk of disease with ageing. We also demonstrate that elastin is preferentially localised to the IFM, potentially having a role in the capacity for matrix recoil after loading which is necessary for the healthy function of energy-storing tendons (Godinho et al., 2017; Ritty et al., 2002). Further supporting a role for elastin in the energy-storing function, elastin appears to be redundant in positional tendons with its abundance decreasing in the CDET with development. Together, these findings show that structural adaptation of tendon post loading is primarily focused to the IFM, and observed predominantly in the energy-storing SDFT.

Compositional analysis of the energy-storing SDFT compartments using mass spectrometry corroborates the immunohistochemical analysis and shows a more complex proteomic profile for the IFM. It additionally shows that abundance of the majority of proteins in the fascicles is higher in the foetus and reduces through development with minimal changes following the initiation of loading, whereas in the IFM numerous ECM and ECM-related proteins progressively increase in abundance following tendon loading and through development.

Neopeptide analysis demonstrated ECM protein turnover in the fascicles slows down towards the end of maturation, whilst ECM protein turnover rates in the IFM are maintained. Once a tendon is mature, little collagen turnover occurs (Birch, 2007; Heinemeier et al., 2013) and we have previously shown that the minimal turnover in mature tendon is focused to the IFM (Simpson et al., 2020; Thorpe et al., 2010; Thorpe, Chaudhry, et al., 2015; Thorpe, Peffers, et al., 2016). The maintenance of turnover rates observed in the IFM here suggests structural and/or compositional plasticity of the IFM. Integrated, our data convincingly show a continual temporal change in the IFM proteome specifically, which would enable adaptation and specialisation to the load environment, and highlight the compositional plasticity of the IFM in responding to dynamic altered conditions such as those occurring during development and regeneration. It is critical that the difference in capacity for functional adaptation across IFM and fascicle identified here is considered if regenerative medicine and tissue engineering approaches are to be successful. Here, we demonstrate the temporal pattern of structure-function adaptation, with compositional changes occurring in the first months after loading, and leading to the mechanical specialisation we have previously observed in adult energy-storing tendon (Birch, 2007; Thorpe et al., 2012; Thorpe, Godinho, et al., 2015). With the fascicles primarily responsible for the mechanical strength of a tissue, biomaterial and regenerative medicine studies have unsurprisingly placed considerable emphasis on this region to date (Sensini et al., 2019; Watts et al., 2017). Here, we not only highlight the importance of the IFM in modulating mechanical behaviour, but also demonstrate how the IFM must be targeted to support adaptation and optimum tissue quality.

Finally, pathway analysis of our proteomic data highlighted TGF-β1 as a regulator of ECM organisation and functional adaptation, predicted to be upregulated following loading in the energy-storing tendon. TGF-β is a known regulator of proteoglycans and collagens in tendon (Potter et al., 2017; Robbins et al., 1997), a role we also demonstrated here with regulation of

major ECM proteins mRNA expression following TGFB1 knockdown and stimulation in equine tenocytes. Further, TGFB1 mRNA expression was upregulated in the highly loaded energy-storing tendon only, supporting the hypothesis that TGF-β1 regulation is specific to the energy-storing tendon and subsequently indicating that it may specifically be associated with loading. Exploring the specificity of TGF-β1 regulation and loading is challenging. Muscle paralysis interventions can be used to demonstrate a causal effect between mechanical force and TGF-β regulation (Subramanian et al., 2018) however such experiments cannot be conducted in horses and other large mammals.

Whilst we acknowledge that other extrinsic factors may drive the changes, our direct comparison of the highly loaded SDFT with the low load CDET enables us to identify that the divergence in mechanical properties, adaptation, and TGF-β regulation all occurs only in the tendon experiencing significant loading. In addition, TGF-β has been shown to have a role in cellular mechanobiology and connective tissue homeostasis, regulating ECM synthesis and remodelling in a force-dependent way following mechanical stimulation, to specify the quality of the ECM and help coordinate cytoskeletal tension (Maeda et al., 2011; Subramanian et al., 2018). A previous study of developing chick tendon detected TGF-β1 staining in the IFM only, during development, highlighting its localised distribution in development (Kuo et al., 2008). In the current study, we are able to associate TGF-β expression also with functional adaptation of the tendon IFM. In addition to tissue development and homeostasis, TGF-β1 is involved in connective tissue injury and repair with abnormal expression levels reported in both processes suggesting a pleiotropic mode of action (Gao et al., 2019). The above may suggest a role for TGF-β1 in tissue development and homeostasis and that its dysregulation is associated with tissue injury and repair.

Outlook

We demonstrate for the first time that functional adaptation in tendon is predominantly reliant on adaptation of the metabolically active IFM, which responds to the mechanical environment through TGF-β signalling, resulting in modulations in ECM turnover and composition to fine-tune mechanical properties. Traditionally, the non-collagenous matrix phase of connective tissues has received considerably less attention than the fibre phase, with regenerative medicine, biomimetics and biomechanics studies all largely focused on investigating and recapitulating the organisation and mechanical properties of the collagenous fibrous network.

Following tendon injury, normal tissue architecture is not recovered, and in particular, the cellular IFM is not regenerated. There is great potential gain from understanding the convergence of biology underpinning adaptation, function and pathology and here, we propose a paradigm shift to consider the metabolically active IFM as a key target for regenerative medicine strategies aimed at addressing functional impairment of tendons and other connective tissues following disease. Regeneration of the IFM following tendon injury could be key for tendon health and low re-injury risk.

Materials and Methods

Key Resources Table				
Reagent type (species) or resource	**Designation**	**Source or reference**	**Identifiers**	**Additional information**
biological sample (*Equus caballus*)	Superficial digital flexor tendon and common digital extensor tendon	Equine practices and commercial abattoir		Foetus-2 years old

biological sample (*Equus caballus*)	Primary superficial digital flexor tendon tenocytes	Commercial abattoir		P3 from adult specimens
antibody	anti-decorin (mouse IgG)	other		(1:1500), Prof. Caterson, Cardiff University, UK
antibody	anti-proteoglycan 4 (mouse IgG)	other		(1:200), Prof. Caterson, Cardiff University, UK
antibody	anti-fibromodulin (rabbit IgG)	other		(1:400), Prof. Roughley, McGill University, Canada
antibody	anti-tenascin C (mouse IgG)	Santa Cruz Biotechnology	RRID:AB_785991	(1:250)
antibody	anti-elastin (mouse IgG)	Abcam	RRID:AB_2099589	(1:250)
antibody	Zytochem Plus HRP polymer anti-mouse	Zytomed systems	RRID:AB_2868565	(75 µL)
antibody	Zytochem Plus HRP polymer anti-rabbit	Zytomed systems	RRID:AB_2868566	(75 µL)
sequenced-based reagent	*Equus caballus* TGFB1 Accell SMARTpool	Dharmacon, Horizon Discovery	https://horizondiscovery.com/en/products/tools/Custom-SMARTpool	(1 µM)
sequenced-based reagent	*Equus caballus* Accell Non-targeting siRNA	Dharmacon, Horizon Discovery	https://horizondiscovery.com/en/products/tools/Custom-SMARTpool	(1 µM)

peptide, recombinant protein	Recombinant Human TGF-β1	Peprotech	100-21	(10 ng/mL)
commercial assay or kit	FASTIN™ Elastin Assay	Biocolor	https://www.biocolor.co.uk/product/fastin-elastin-assay/	
chemical compound, drug	RapiGest SF	Waters	https://www.waters.com/waters/en_GB/RapiGest-SF-Surfactant/	(0.1% w/v)
software, algorithm	HistoQuest Analysis Software	Tissuegnostics	RRID:SCR_014823	
software, algorithm	Adobe Photoshop CS3	Adobe	RRID:SCR_014199	
software, algorithm	Peaks Studio v8.5	Bioinformatics Solutions	www.bioinfor.com/peaks-studio	
software, algorithm	Ingenuity Pathway Analysis	Qiagen	RRID:SCR_008653	
software, algorithm	Matrisome	PMID: 2197732	http://matrisomeproject.mit.edu	
software, algorithm	Mascot	Matrix Science	RRID:SCR_014322	
software, algorithm	Neopeptide Analyser	PMID: 28503667	https://github.com/PGB-LIV/neo-pep-tool/releases/	
software, algorithm	SigmaPlot	Systat Software Inc	RRID:SCR_003210	
software, algorithm	GProX	PMID: 21602510	RRID:SCR_000273	
other	Chondroitinase ABC from *Proteus vulgaris*	Merck	C2509	(0.2 U/mL)

other	Hyaluronidase from bovine testes	Merck	H3506	(4800 U/mL)

Experimental design

Using an equine tendon model, we investigate the process and drivers of functional adaptation in the SDFT and CDET, two functionally distinct tendons, when tendons transition from an absence of loading (foetal: mid to end (6 to 9 months) gestation, and 0 days: full-term foetuses, and foals that did not weight-bear); through to weight-bearing (0-1 month) and then to an increase in body weight and physical activity (3-6 months; and 1-2 years). We use a phase-specific approach to characterise each tendon phase independently, by comparing fascicles (fibre phase) and interfascicular matrix (IFM; matrix phase) mechanical properties, structure and composition.

For this purpose, we used mechanical testing, histological and immunohistochemical analysis and mass spectrometry analysis following laser capture microdissection. Sample size was selected based on previous experiments and restricted by sample availability and the cost of mass spectrometry analysis.

Sample collection

Both forelimbs were collected from foetuses and foals aged 0-2 years (n=19) euthanised for reasons unrelated to this project at a commercial abattoir or equine practices following owner consent under ethical approval for use of the cadaveric material granted by the Veterinary Research Ethics Committee, School of Veterinary Science, University of Liverpool (VREC352). Collected tendons were split in the following age groups: Foetus (between 6 and 9 months of gestation; n=4); 0 days (full-term foetuses (average gestation 11-12 months) and foals that did not weight-bear; n=4): 0-1 month (n=3); 3-6 months (n=4); 1-2 years (n=4).

The SDFT and CDET from one forelimb were dissected and wrapped in phosphate-buffered saline dampened tissue paper and foil and stored at -80 ^{o}C for biomechanical testing. Two 1-2 cm segments from the mid-metacarpal area of the SDFT and CDET of the other forelimb were dissected, and one fixed in 4% paraformaldehyde for histology and immunohistochemistry, and the other snap frozen in isopentane and stored at -80 ^{o}C for laser capture microdissection.

Biomechanical testing of the fascicles

On the day of testing, samples were defrosted within their tissue paper wrap, then immediately prepared for testing. Fascicles were dissected from the mid-metacarpal region of the SDFT and CDET and subjected to a quasi-static test to failure according to Thorpe et al. (2015) (Thorpe, Godinho, et al., 2015). Briefly, prior to testing, the diameter of each fascicle was measured along a 1 cm length in the middle of the fascicle with a non-contact laser micrometre (LSM-501, Mitotuyo, Japan, resolution = 0.5 μm) and the smallest diameter recorded and used to calculate cross-sectional area (CSA), assuming a circular shape.

Fascicles were loaded in an electrodynamic testing machine (Instron ElectroPuls 1000) equipped with a 250 N load cell and pneumatic grips (4 bar) coated with rubber and sandpaper to prevent sample slippage (Thorpe et al., 2012). The distance between the grips was set to 20 mm and fascicles preloaded to 0.1 N (approx. 2% fascicle failure load) to remove any slack in the sample. Following preload, the distance between the grips was recorded as the gauge length, then fascicles preconditioned with 10 loading cycles between 0 and 3% strain (approximately 25% failure strain) using a sine wave at 1 Hz frequency. Immediately after preconditioning, fascicles were pulled to failure at a strain rate of 5%/s. Force and extension data were continuously recorded at 100 Hz during both preconditioning and the quasi-static test to failure. Acquired data were smoothed to reduce noise before

calculations with a 3rd order Savitzky-Golay low pass filter, with a frame of 15 for the preconditioning data and 51 for the pull to failure data.

Using the preconditioning data, the total percentage hysteresis and stress relaxation were calculated, between the first and last preconditioning cycle. Failure force, extension, stress, and strain were calculated from the test to failure, and a continuous modulus calculated across every 10 data points of each stress strain curve, from which the maximum modulus value was determined. The point of maximum modulus was defined as the yield point from which yield stress and yield strain were determined.

Biomechanical testing of the IFM

On the day of testing, tendons were defrosted within their tissue paper wrap, and IFM samples immediately dissected and prepared for biomechanical testing as described previously by Thorpe et al. (2012) (Thorpe et al., 2012). Briefly, a group of two adjacent intact fascicles (bound by the IFM) were dissected, after which the opposing end of each fascicle was cut transversely 10 mm apart, to leave a consistent 10 mm length of intact IFM that could be tested in shear (Figure 1 – Figure supplement 1c).

Utilising the same electrodynamic testing machine and pneumatic grips as described for the fascicles, the intact end of each fascicle was gripped with a grip to grip distance of 20 mm, and a pre-load of 0.02 N (approx. 1% IFM failure load) applied. IFM samples were preconditioned with 10 cycles between 0 and 0.5 mm extension (approx. 25% failure extension) using a sine wave at 1 Hz frequency, then pulled to failure at a speed of 1 mm/s. Force and extension data were continuously recorded at 100 Hz during both preconditioning and the quasi-static test to failure. Acquired data was smoothed to reduce noise before calculations with a 3rd order Savitzky-Golay low pass filter, with a frame of 15 for the preconditioning data and 51 for the pull to failure data.

Total percentage hysteresis and stress relaxation were again calculated between the first and last preconditioning cycle. Failure force and extension were determined from the quasi-static pull to failure curve, and a continual stiffness curve was calculated across every 10 data points of the curve, from which maximum stiffness was determined, and yield force and yield extension at maximum stiffness reported. Based on previous data demonstrating notable differences in the toe region of the IFM curve of functionally distinct tendons, the shape of failure curves was also compared between samples by calculating the amount of IFM extension at different percentages of IFM failure load (Thorpe, Godinho, et al., 2015).

Histology scoring

Paraformaldehyde-fixed paraffin-embedded longitudinal SDFT and CDET segments were sectioned at 6 μm thickness and stained with H&E for histologic examination and scoring (n=13; 3 from each age group, 4 from 1-2 years age group). The examined histologic variables are reported in Supplementary File 1 and adapted from Nixon et al. 2008 (Nixon et al., 2008).

For parameters scored by investigators, the sections were blinded and histologic variables assigned a grade from 0 to 3 by two independent investigators. Weighted Kappa showed moderate to good agreement in all instances, hence the average of the two scores was used. Other histologic variables were measured using image analysis (HistoQuest Analysis software, RRID:SCR_014823, Tissuegnostics and Adobe Photoshop CS3, RRID:SCR_014199) and then assigned a grade from 0 to 3. Cumulative scores for the fascicle and IFM for each horse were obtained by summing the scores of the fascicle and IFM variables, respectively, excluding IFM percentage to ensure IFM dimensions were not over-weighted in final reporting.

Immunohistochemistry

Immunohistochemical analysis for DCN, FMOD, PRG4, TNC and ELN was carried out on paraformaldehyde-fixed paraffin-embedded longitudinal SDFT and CDET sections (6 µm thickness) (n=12; 3 from each age group) as previously described by Zamboulis et al. (2013) (Zamboulis et al., 2013). Antigen retrieval was carried out with 0.2 U/mL Chondroitinase ABC (C2905, Sigma, Merck, Darmstadt, Germany) at 37 ^{o}C for two hours for DCN, FMOD, PRG4, and TNC or with 4800 U/mL hyaluronidase (H3506, Sigma, Merck, Darmstadt, Germany) at 37 ^{o}C for two hours for ELN. Primary antibodies were used at a concentration of 1:1500 for DCN (mouse IgG), 1:400 for FMOD (rabbit IgG), 1:200 for PRG4 (mouse IgG), 1:250 for TNC (mouse IgG, RRID:AB_785991, Santa Cruz Biotechnology, Dallas, Texas), and 1:100 for ELN (mouse IgG, RRID:AB_2099589, Abcam, Cambridge, UK). Antibodies for DCN and PRG4 were a kind gift from Prof. Caterson, Cardiff University, UK, and the FMOD antibody was kindly provided by Prof. Roughley, McGill University, Canada. The secondary antibody incubation was performed with the Zytochem Plus HRP Polymer anti-rabbit for FMOD and anti-mouse for DCN, PRG4, TNC, and ELN (RRID:AB_2868566 and RRID:AB_2868565, Zytomed Systems, Berlin, Germany). Immunohistochemical staining was graded from 0 to 3 (low to high) on blinded sections, assessing stained area and staining intensity for DCN, FMOD, TNC, and ELN. For PRG4, where staining was confined to the pericellular area, staining intensity was measured using HistoQuest Analysis software (Tissuegnostics, RRID:SCR_014823).

Quantification of tendon elastin

The elastin content of SDFT and CDET samples from each age group (n=12; 3 from each age group) was quantified using the FASTIN^{TM} Elastin Assay (Biocolor, Carrickfergus, UK) (Godinho et al., 2017). Briefly, SDFT and CDET tissue was powdered (~15 mg wet weight) and incubated with 750 µl of 0.25 M oxalic acid at 100 °C for 2 one hour cycles to extract all soluble a-elastin from the tissue. Preliminary tests showed two extractions were

598 sufficient to solubilise all a-elastin from developing SDFT and CDET. Following
599 extraction, samples and standards were processed in duplicate according to the
600 manufacturer's instructions and their absorbance determined spectrophotometrically at
601 513 nm (Spectrostar Nano microplate reader, BMG Labtech, Aylesbury, UK). A standard
602 curve was used to calculate the samples' elastin concentration and elastin was expressed as
603 a percentage of tendon wet weight.

604 **Laser-capture microdissection**

605 Laser-capture microdissection was used to collect samples from the fascicles and IFM of
606 SDFT samples from all age groups (n=4 for each age group with the exception of the 0-1
607 month group where n=3). For this purpose, 12 µm transverse cryosections were cut from the
608 SDFT samples and mounted on steel frame membrane slides (1.4 µm PET membrane, Leica
609 Microsystems, Wetzlar, Germany). Frozen sections were dehydrated in 70% and 100% ice-
610 cold ethanol, allowed to briefly dry, and regions of fascicle and IFM laser-captured on an
611 LMD7000 laser microdissection microscope (Leica Microsystems, Wetzlar, Germany) and
612 collected in LC/MS grade water (FisherScientific, Hampton, New Hampshire). Collected
613 samples were immediately snap frozen and stored at -80 ^{o}C for mass spectrometry analysis.

614 **Mass spectrometry analysis**

615 Mass spectrometry analysis of laser-captured SDFT fascicle and IFM samples was carried out
616 as previously described by Thorpe et al. (2016) (Thorpe, Peffers, et al., 2016). Samples were
617 digested for mass spectrometry analysis with incubation in 0.1% (w/v) Rapigest (Waters,
618 Herts, UK) for 30 min at room temperature followed by 60 min at 60 °C and subsequent
619 trypsin digestion. LC MS/MS was carried out at the University of Liverpool Centre for
620 Proteome Research using an Ultimate 3000 Nano system (Dionex/Thermo Fisher Scientific,
621 Waltham, Massachusetts) for peptide separation coupled online to a Q-Exactive Quadrupole-

Orbitrap mass spectrometer (Thermo Scientific, Waltham, Massachusetts) for MS/MS acquisition. Initial ranging runs on short gradients were carried out to determine the sample volume to be loaded on the column and subsequently between 1-9 µL of sample was loaded onto the column on a one hour gradient with an inter-sample 30 min blank.

Protein identification and label-free quantification

Fascicle and IFM proteins were identified using Peaks® 8.5 PTM software (Bioinformatics Solutions, Waterloo, Canada), searching against the UniHorse database (http://www.uniprot.org/proteomes/). Search parameters used were: peptide mass tolerance 10 ppm, fragment mass tolerance 0.01 Da, fixed modification carbamidomethylation, variable modifications methionine oxidation and hydroxylation. Search results for peptide identification were filtered with a false discovery rate (FDR) of 1%, and for protein identification with a minimum of 2 unique peptides per protein, and a confidence score >20 (-10lgp>20). Label-free quantification was also carried out using Peaks® 8.5 PTM software for the SDFT fascicle and IFM separately. Protein abundances were normalised for collected laser-capture area and volume loaded onto the mass spectrometry column and differentially abundant proteins between the age groups in the SDFT fascicle and IFM were identified using a fold change ≥2 and $p<0.05$ (PEAKS adjusted p values). The mass spectrometry proteomics data have been deposited to the ProteomeXchange Consortium via the PRIDE partner repository, with the dataset identifier PXD012169 and 10.6019/PXD012169. With the IFM showing changes both in its protein composition and mechanical properties during development and TGFB1 being linked to protein composition, differentially expressed matrisome proteins identified in the IFM were correlated to TGFB1 whole tendon mRNA expression and the IFM mechanical properties using the Pearson correlation coefficient ($p<0.05$).

Gene ontology and network analysis

The dataset of identified proteins in the SDFT fascicles and IFM were classified for cell compartment association with the Ingenuity Pathway Analysis software (IPA, RRID:SCR_008653, Qiagen, Hilden, Germany) and for matrisome categories with The Matrisome Project database (Hynes & Naba, 2012). Protein pathway analysis for the differentially abundant proteins between age groups in the SDFT fascicle and IFM was carried out in IPA. Protein interactions maps were created in IPA allowing for experimental evidence and highly predicted functional links.

Neopeptide identification

For neopeptide identification, mass spectrometry data was analysed using Mascot server (Matrix Science, RRID:SCR_014322) with the search parameters: enzyme semiTrypsin, peptide mass tolerance 10 ppm, fragment mass tolerance 0.01 Da, charge 2+ and 3+ ions, and missed cleavages 1. The included modifications were: fixed carbamidomethyl cysteine, variables oxidation of methionine, proline, and lysine, and the instrument type selected was electrospray ionization-TRAP (ESI-TRAP). The Mascot-derived ion score was used to determine true matches ($p<0.05$), where p was the probability that an observed match was a random event. The peptide list was exported and processed with the Neopeptide Analyser, a software tool for the discovery of neopeptides in proteomic data (Peffers et al., 2017). Obtained neopeptide abundances for each sample were normalised for total peptide abundance for that protein and sample, and normalised neopeptide abundances were subsequently summed for each protein and the total neopeptide abundance analysed for differential abundance across the age groups in the SDFT fascicles and IFM using $p<0.05$ and FDR 5% (ANOVA and Benjamini-Hochberg FDR).

Relative mRNA expression

Laser capture microdissection collects very small amounts of tissue which is not adequate for mRNA expression analysis and therefore whole tendon was used for the mRNA expression analysis. RNA extraction from whole SDFT and CDET was carried out followed by reverse transcription. Quantitative real-time PCR (qRT-PCR) was performed on an ABI7300 system (Thermo Fisher Scientific Waltham, Massachusetts) using the Takyon ROX SYBR 2X MasterMix (Eurogentec, Liege, Belgium). qRT-PCR was undertaken using previously validated gene-specific primers for DCN, FMOD, BGN, COMP, COL1A1, COL1A2, COL3A1, TGFB1, and GAPDH as a reference gene (Peffers et al., 2013; Taylor et al., 2009) (Supplementary File 2). Relative expression levels were normalised to GAPDH expression and calculated with the formula $E^{-\Delta Ct}$ following primer efficiency calculation.

SiRNA TGFB1 silencing and TGFb1 addition in tenocytes

Tenocytes isolated from young adult SDFT (passage 3, n=4, average age: 5 years old) were transfected with custom Accell equine TGFB1 siRNA pool and an Accell non-targeting siRNA (Dharmacon, Horizon Discovery Ltd, Cambridge, UK) for 4 days to silence TGFB1. Experiments were carried out in the following 24 hours once TGFB1 knockdown was satisfactory. For TGFB1 stimulation, 10 ng/mL recombinant human TGFB1 (Peprotech, Cranbury, USA) was added to equine tenocytes for 24 hours, whilst control cells were incubated in the same media without any additions. qRT-PCR was undertaken as described above, using previously validated gene-specific primers for TGFB1, BGN, COMP, DCN, ASPN, FBLN5, COL1A2, COL3A1, and RPS20 as a reference gene (Peffers et al., 2013; Taylor et al., 2009) (Supplementary File 2).

Statistical analysis

Statistical analysis was carried out in SigmaPlot (RRID:SCR_003210, Systat Software Inc, San Jose, California) unless otherwise stated. Details of the n numbers for each experiment

and the statistical test used for the analysis of the data are listed in Supplementary File 3. Heatmaps were designed in GProX (RRID:SCR_000273) (Rigbolt et al., 2011). The Central Limit Theorem (CLT) was used to assume normality where n>30 and where n<30 normality was tested using the Shapiro-Wilks test. If data were found not to be normally distributed their log10 transformation or ANOVA on Ranks was used for statistical analysis but the original data was presented in graphs.

Acknowledgements

This work was funded by the Horserace Betting Levy Board, PRJ/776. We would like to acknowledge the equine practices that provided samples for this study.

Author Contributions

DEZ designed and performed experiments, analysed the data, and wrote the manuscript. CTT assisted with study design, data analysis, and edited the manuscript. YAK assisted with data collection and analysis. HLB, HRCS, PDC conceived the study, assisted with data analysis, and edited the manuscript.

Competing Interests statement

The authors declare that they have no competing interests.

Data and materials availability

The mass spectrometry proteomics data have been deposited to the ProteomeXchange Consortium via the PRIDE partner repository, with the dataset identifier PXD012169 and 10.6019/PXD012169.

References

Alexander, R. M. N. (2002). Tendon elasticity and muscle function. *Comparative Biochemistry and Physiology - A Molecular and Integrative Physiology*, *133*(4), 1001–1011. https://doi.org/10.1016/S1095-6433(02)00143-5

Ansorge, H. L., Adams, S., Birk, D. E., & Soslowsky, L. J. (2011). Mechanical, compositional, and structural properties of the post-natal mouse Achilles tendon. *Annals of Biomedical Engineering*, *39*(7), 1904–1913. https://doi.org/10.1007/s10439-011-0299-0

Armiento, A. R., Stoddart, M. J., Alini, M., & Eglin, D. (2018). Biomaterials for articular cartilage tissue engineering: Learning from biology. *Acta Biomaterialia*, *65*, 1–20. https://doi.org/10.1016/j.actbio.2017.11.021

Batson, E. L., Paramour, R. J., Smith, T. J., Birch, H. L., Patterson-Kane, J. C., & Goodship, A. E. (2003). Are the material properties and matrix composition of equine flexor and extensor tendons determined by their functions? *Equine Veterinary Journal*, *35*(3), 314–318. https://doi.org/10.2746/042516403776148327

Biewener, A. A. (1998). Muscle-tendon stresses and elastic energy storage during locomotion in the horse. *Comparative Biochemistry and Physiology - B Biochemistry and Molecular Biology*, *120*(1), 73–87. https://doi.org/10.1016/S0305-0491(98)00024-8

Birch, H. L. (2007). Tendon matrix composition and turnover in relation to functional requirements. *International Journal of Experimental Pathology*, *88*(4), 241–248. https://doi.org/10.1111/j.1365-2613.2007.00552.x

740 Birch, H. L., Worboys, S., Eissa, S., Jackson, B., Strassburg, S., & Clegg, P. D. (2008).
741 Matrix metabolism rate differs in functionally distinct tendons. *Matrix Biology*, *27*(3),
742 182–189. https://doi.org/10.1016/j.matbio.2007.10.004
743 Cherdchutham, W., Becker, C. K., Spek, E. R., Voorhout, W. E., & Van Weeren, P. R.
744 (2001). Effects of exercise on the diameter of collagen fibrils in the central core and
745 periphery of the superficial digital flexor tendon in foals. *American Journal of*
746 *Veterinary Research*, *62*(10), 1563–1570. https://doi.org/10.2460/ajvr.2001.62.1563
747 Cherdchutham, W., Meershoek, L. S., Weeren, P. R. Van, & Barneveld, A. (2001). Effects of
748 exercise on biomechanical properties of the superficial digital flexor tendon in foals.
749 *American Journal of Veterinary Research*, *62*(12), 1859–1864. https://avmajournals-
750 avma-org.proxy1.cl.msu.edu/doi/pdf/10.2460/ajvr.2001.62.1859
751 Choi, R. K., Smith, M., Clarke, E., & Little, C. (2018). Cellular, matrix, and mechano-
752 biological differences in load-bearing versus positional tendons throughout development
753 and aging: a narrative review. *Connective Tissue Research*, *59*(5), 483–494.
754 https://doi.org/10.1080/03008207.2018.1504929
755 Choi, R. K., Smith, M. M., Smith, S., Little, C. B., & Clarke, E. C. (2019). Functionally
756 distinct tendons have different biomechanical, biochemical and histological responses to
757 in vitro unloading. *Journal of Biomechanics*, *95*, 109321.
758 https://doi.org/10.1016/j.jbiomech.2019.109321
759 Freedman, B. R., Bade, N. D., Riggin, C. N., Zhang, S., Haines, P. G., Ong, K. L., & Janmey,
760 P. A. (2015). The (dys)functional extracellular matrix. *Biochimica et Biophysica Acta -*
761 *Molecular Cell Research*, *1853*(11), 3153–3164.
762 https://doi.org/10.1016/j.bbamcr.2015.04.015
763 Gao, F., Li, C., Zhou, J., Shen, X., Hu, B., Lu, M., Liu, Y., Zhang, B., Fang, Y., & Liu, Y.
764 (2019). Progress on relationship between transforming growth factor-beta1 and

765 tendinopathy. *China Journal of Orthopaedics and Traumatology*, *32*(4), 377–382.
766 Gardner, K., Arnoczky, S. P., Caballero, O., & Lavagnino, M. (2008). The effect of stress-
767 deprivation and cyclic loading on the TIMP/MMP ratio in tendon cells: An in vitro
768 experimental study. *Disability and Rehabilitation*, *30*(20–22), 1523–1529.
769 https://doi.org/10.1080/09638280701785395
770 Godinho, M. S. C., Thorpe, C. T., Greenwald, S. E., & Screen, H. R. C. (2017). Elastin is
771 Localised to the Interfascicular Matrix of Energy Storing Tendons and Becomes
772 Increasingly Disorganised With Ageing. *Scientific Reports*, *7*(1), 1–11.
773 https://doi.org/10.1038/s41598-017-09995-4
774 Heinemeier, K. M., Schjerling, P., Heinemeier, J., Magnusson, S. P., & Kjaer, M. (2013).
775 *Lack of tissue renewal in human adult Achilles tendon is revealed by nuclear bomb 14C*
776 (pp. 2074–2079).
777 Hynes, R. O., & Naba, A. (2012). Overview of the matrisome-An inventory of extracellular
778 matrix constituents and functions. *Cold Spring Harbor Perspectives in Biology*, *4*(1), 1–
779 16. https://doi.org/10.1101/cshperspect.a004903
780 Kalson, N. S., Holmes, D. F., Herchenhan, A., Lu, Y., Starborg, T., & Kadler, K. E. (2011).
781 Slow stretching that mimics embryonic growth rate stimulates structural and mechanical
782 development of tendon-like tissue in vitro. *Developmental Dynamics*, *240*(11), 2520–
783 2528. https://doi.org/10.1002/dvdy.22760
784 Kohrs, R. T., Zhao, C., Sun, Y. L., Jay, G. D., Zhang, L., Warman, M. L., An, K. N., &
785 Amadio, P. C. (2011). Tendon fascicle gliding in wild type, heterozygous, and lubricin
786 knockout mice. *Journal of Orthopaedic Research*, *29*(3), 384–389.
787 https://doi.org/10.1002/jor.21247
788 Kostrominova, T. Y., & Brooks, S. V. (2013). Age-related changes in structure and
789 extracellular matrix protein expression levels in rat tendons. *Age*, *35*(6), 2203–2214.

https://doi.org/10.1007/s11357-013-9514-2

Kuo, C., Petersen, B., & Tuan, R. (2008). Spatiotemporal protein distribution of TGF-ß's, their receptors, and extracellular matrix molecules during embryonic tendon development. *Developmental Dynamics*, *237*(5), 1477–1489. https://doi.org/10.1002/dvdy.21547.Spatiotemporal

Maeda, T., Sakabe, T., Sunaga, A., Sakai, K., Rivera, A. L., Keene, D. R., Sasaki, T., Stavnezer, E., Iannotti, J., Schweitzer, R., Ilic, D., Baskaran, H., & Sakai, T. (2011). Conversion of mechanical force into TGF-β-mediated biochemical signals. *Current Biology*, *21*(11), 933–941. https://doi.org/10.1016/j.cortex.2009.08.003.Predictive

Magnusson, S. P., & Kjaer, M. (2019). The impact of loading, unloading, ageing and injury on the human tendon. *Journal of Physiology*, *597*(5), 1283–1298. https://doi.org/10.1113/JP275450

Marturano, J. E., Arena, J. D., Schiller, Z. A., Georgakoudi, I., & Kuo, C. K. (2013). Characterization of mechanical and biochemical properties of developing embryonic tendon. *Proceedings of the National Academy of Sciences of the United States of America*, *110*(16), 6370–6375. https://doi.org/10.1073/pnas.1300135110

Mendias, C. L., Gumucio, J. P., & Lynch, E. B. (2012). Mechanical loading and TGF-β change the expression of multiple miRNAs in tendon fibroblasts. *Journal of Applied Physiology*, *113*(1), 56–62. https://doi.org/10.1152/japplphysiol.00301.2012

Nixon, A. J., Dahlgren, L. A., Haupt, J. L., Yeager, A. E., & Ward, D. L. (2008). Effect of adipose-derived nucleated cell fractions on tendon repair in horses with collagenase-induced tendinitis. *American Journal of Veterinary Research*, *69*(7).

Pan, X. S., Li, J., Brown, E. B., & Kuo, C. K. (2018). Embryo movements regulate tendon mechanical property development. *Philosophical Transactions of the Royal Society B: Biological Sciences*, *373*(1759). https://doi.org/10.1098/rstb.2017.0325

Patterson-Kane, J. C., & Rich, T. (2014). Achilles tendon injuries in elite athletes: Lessons in pathophysiology from their equine Counterparts. *ILAR Journal*, *55*(1), 86–99. https://doi.org/10.1093/ilar/ilu004

Peffers, M. J., Jones, A. R., McCabe, A., & Anderson, J. (2017). Neopeptide Analyser: A software tool for neopeptide discovery in proteomics data. *Wellcome Open Research*, *2*(May), 1–9. https://doi.org/10.12688/wellcomeopenres.11275.1

Peffers, M. J., Liu, X., & Clegg, P. D. (2013). Transcriptomic signatures in cartilage ageing. *Arthritis Research and Therapy*, *15*(4), R98. https://doi.org/10.1186/ar4278

Potter, R. M., Huynh, R. T., Volper, B. D., Arthur, K. A., D'Lugos, A. C., Sørensen, M. A., Peter Magnusson, S., Dickinson, J. M., Hale, T. M., & Carroll, C. C. (2017). Impact of TGF-β inhibition during acute exercise on achilles tendon extracellular matrix. *American Journal of Physiology - Regulatory Integrative and Comparative Physiology*, *312*(1), R157–R164. https://doi.org/10.1152/ajpregu.00439.2016

Rigbolt, K. T. G., Vanselow, J. T., & Blagoev, B. (2011). GProX, a user-friendly platform for bioinformatics analysis and visualization of quantitative proteomics data. *Molecular and Cellular Proteomics*, *10*(8), 1–10. https://doi.org/10.1074/mcp.O110.007450

Ritty, T. M., Ditsios, K., & Starcher, B. C. (2002). Distribution of the elastic fiber and associated proteins in flexor tendon reflects function. *Anatomical Record*, *268*(4), 430–440. https://doi.org/10.1002/ar.10175

Robbins, J. R., Evanko, S. P., & Vogel, K. G. (1997). Mechanical loading and TGF-β regulate proteoglycan synthesis in tendon. *Archives of Biochemistry and Biophysics*, *342*(2), 203–211. https://doi.org/10.1006/abbi.1997.0102

Russo, V., Mauro, A., Martelli, A., Di Giacinto, O., Di Marcantonio, L., Nardinocchi, D., Berardinelli, P., & Barboni, B. (2015). Cellular and molecular maturation in fetal and adult ovine calcaneal tendons. *Journal of Anatomy*, *226*(2), 126–142.

https://doi.org/10.1111/joa.12269

Sensini, A., Gualandi, C., Focarete, M., Belcari, J., Zucchelli, A., Boyle, L., Reilly, G., Kao, A., Tozzi, G., & Cristofolini, L. (2019). Multiscale hierarchical bioresorbable scaffolds for the regeneration of tendons and ligaments. *Biofabrication*, *11*(3), 035026.

Simpson, D., Choi, H., Wang, D., Prescott, M., Pitsillides, A. A., Dudhia, J., Clegg, P. D., Ping, P., & Thorpe, C. T. (2020). Heterogeneity of proteome dynamics between connective tissue phases of adult tendon. *ELife*, *9*, 1–29. https://doi.org/10.7554/eLife.55262

Spiesz, E. M., Thorpe, C. T., Chaudhry, S., Riley, G. P., Birch, H. L., Clegg, P. D., & Screen, H. R. C. (2015). Tendon extracellular matrix damage, degradation and inflammation in response to in vitro overload exercise. *Journal of Orthopaedic Research*, *33*(6), 889–897. https://doi.org/10.1002/jor.22879

Stanley, R. L., Edwards, L. J., Goodship, A. E., Firth, E. C., & Patterson-Kane, J. C. (2008). Effects of exercise on tenocyte cellularity and tenocyte nuclear morphology in immature and mature equine digital tendons. *Equine Veterinary Journal*, *40*(2), 141–146. https://doi.org/10.2746/042516408X266097

Subramanian, A., Kanzaki, L. F., Galloway, J. L., & Schilling, T. F. (2018). Mechanical force regulates tendon extracellular matrix organization and tenocyte morphogenesis through TGFbeta signaling. *ELife*, *7*, 1–24. https://doi.org/10.7554/eLife.38069

Subramanian, A., & Schilling, T. F. (2014). Thrombospondin-4 controls matrix assembly during development and repair of myotendinous junctions. *ELife*, *2014*(3), 1–21. https://doi.org/10.7554/eLife.02372

Taye, N., Karoulias, S. Z., & Hubmacher, D. (2020). The “other” 15–40%: The Role of Non-Collagenous Extracellular Matrix Proteins and Minor Collagens in Tendon. *Journal of Orthopaedic Research*, *38*(1), 23–35. https://doi.org/10.1002/jor.24440

Taylor, S. E., Vaughan-Thomas, A., Clements, D. N., Pinchbeck, G., MacRory, L. C., Smith, R. K., & Clegg, P. D. (2009). Gene expression markers of tendon fibroblasts in normal and diseased tissue compared to monolayer and three dimensional culture systems. *BMC Musculoskeletal Disorders*, *10*, 1–10. https://doi.org/10.1186/1471-2474-10-27

Thorpe, C. T., Chaudhry, S., Lei, I. I., Varone, A., Riley, G. P., Birch, H. L., Clegg, P. D., & Screen, H. R. C. (2015). Tendon overload results in alterations in cell shape and increased markers of inflammation and matrix degradation. *Scandinavian Journal of Medicine and Science in Sports*, *25*(4), e381–e391. https://doi.org/10.1111/sms.12333

Thorpe, C. T., Godinho, M. S. C., Riley, G. P., Birch, H. L., Clegg, P. D., & Screen, H. R. C. (2015). The interfascicular matrix enables fascicle sliding and recovery in tendon, and behaves more elastically in energy storing tendons. *Journal of the Mechanical Behavior of Biomedical Materials*, *52*, 85–94. https://doi.org/10.1016/j.jmbbm.2015.04.009

Thorpe, C. T., Karunaseelan, K. J., Ng Chieng Hin, J., Riley, G. P., Birch, H. L., Clegg, P. D., & Screen, H. R. C. (2016). Distribution of proteins within different compartments of tendon varies according to tendon type. *Journal of Anatomy*, *229*(3), 450–458. https://doi.org/10.1111/joa.12485

Thorpe, C. T., Peffers, M. J., Simpson, D., Halliwell, E., Screen, H. R. C., & Clegg, P. D. (2016). Anatomical heterogeneity of tendon: Fascicular and interfascicular tendon compartments have distinct proteomic composition. *Scientific Reports*, *6*(February), 1–12. https://doi.org/10.1038/srep20455

Thorpe, C. T., Riley, G. P., Birch, H. L., Clegg, P. D., & Screen, H. R. C. (2016). Fascicles and the interfascicular matrix show adaptation for fatigue resistance in energy storing tendons. *Acta Biomaterialia*, *42*, 308–315. https://doi.org/10.1016/j.actbio.2016.06.012

Thorpe, C. T., & Screen, H. R. C. (2016). Tendon structure and composition. In *Advances in Experimental Medicine and Biology* (Vol. 920). https://doi.org/10.1007/978-3-319-

33943-6

Thorpe, C. T., Streeter, I., Pinchbeck, G. L., Goodship, A. E., Clegg, P. D., & Birch, H. L. (2010). Aspartic acid racemization and collagen degradation markers reveal an accumulation of damage in tendon collagen that is enhanced with aging. *Journal of Biological Chemistry*, *285*(21), 15674–15681. https://doi.org/10.1074/jbc.M109.077503

Thorpe, C. T., Udeze, C. P., Birch, H. L., Clegg, P. D., & Screen, H. R. C. (2012). Specialization of Tendon Mechanical Properties Results From Interfascicular Differences. *Journal of The Royal Society Interface*, *9*(76), 3108–3117.

Thorpe, C. T., Udeze, C. P., Birch, H. L., Clegg, P. D., & Screen, H. R. C. (2013). Capacity for sliding between tendon fascicles decreases with ageing in injury prone equine tendons: A possible mechanism for age-related tendinopathy? *European Cells and Materials*, *25*(0), 48–60.

Watts, A. E., Millar, N. L., Platt, J., Kitson, S. M., Akbar, M., Rech, R., Griffin, J., Pool, R., Hughes, T., McInnes, I. B., & Gilchrist, D. S. (2017). MicroRNA29a Treatment Improves Early Tendon Injury. *Molecular Therapy*, *25*(10), 2415–2426. https://doi.org/10.1016/j.ymthe.2017.07.015

Zamboulis, D. E., Senior, J. M., Clegg, P. D., Gallagher, J. A., Carter, S. D., & Milner, P. I. (2013). Distribution of purinergic P2X receptors in the equine digit, cervical spinal cord and dorsal root ganglia. *Purinergic Signalling*, *9*(3), 383–393. https://doi.org/10.1007/s11302-013-9356-5

Supplementary data

Figure 1 – Figure supplement 1. SDFT and CDET in the equine forelimb, tendon structure, and schematic showing procedure for biomechanical testing.

Figure 3 – Figure supplement 1. Scoring of histologic variables for the IFM and fascicle in the SDFT and CDET through postnatal development.

Figure 4 – Figure supplement 1. Scoring of ELN staining for the IFM and fascicle in the SDFT and CDET through postnatal development.

Figure 5 – Figure supplement 1. Classification of SDFT IFM and fascicle identified proteins and differentially abundant proteins according to their associated location.

Figure 5 – Figure supplement 2. Relative mRNA expression of major ECM genes in whole tissue SDFT and CDET through postnatal development.

Supplementary File 1. Histologic variables used in the H&E scoring of the SDFT and CDET sections and the analysis method and reporting criteria adopted.

Supplementary File 2. Gene primer sequences used in relative mRNA expression analysis.

Supplementary File 3. Samples used for analysis along with statistical test used for analysis.

Supplementary File 4. Collagens and proteoglycans identified in SDFT IFM and fascicle.

Supplementary File 5. Correlation analysis of IFM protein abundance and mechanical properties across development.

Supplementary File 6. Correlation analysis of TGFB1 whole tendon mRNA expression and IFM protein abundance across development.

Figure 1 and 2 – Source Data 1. Fascicle and IFM mechanical properties.

Table 1 and 2 – Source Data 2. IFM and fascicle matrisome proteins intensity.

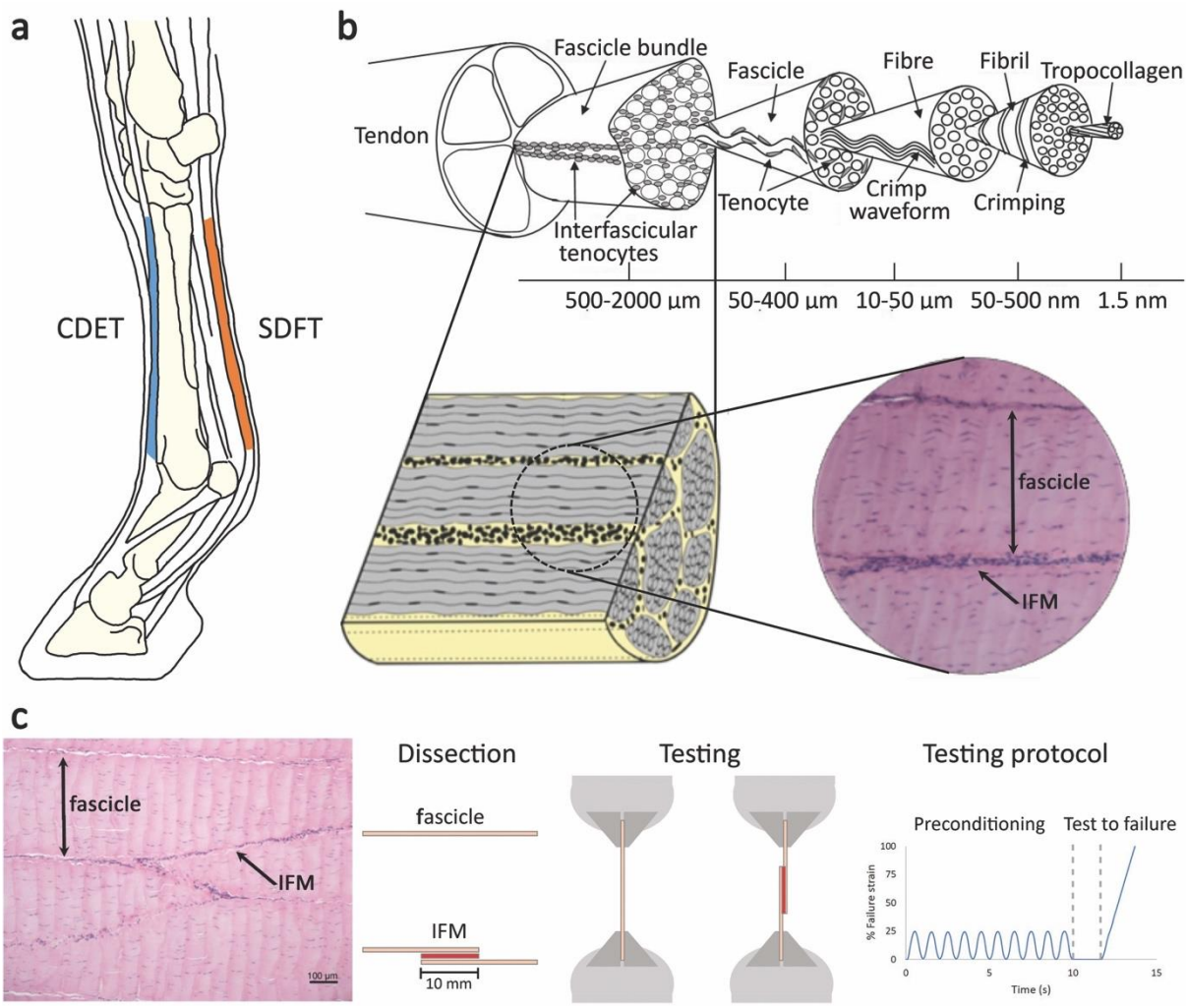

Figure 1 – Figure supplement 1. SDFT and CDET in the equine forelimb, tendon structure, and schematic showing procedure for biomechanical testing. (**a**) Schematic of the equine forelimb with the CDET and SDFT highlighted. (**b**) Tendon structure (partially reproduced from Figure 1, Spiesz et al. 2015, *Journal of Orthopaedic Research*, published under the Creative Commons Attribution 4.0 International Public License (CC BY 4.0; https://creativecommons.org/licenses/by/4.0/). (**c**) H&E section of fascicle and IFM and schematic of fascicle and IFM dissection and biomechanical testing.

IFM	Scoring	Fascicle	Scoring
Percentage of IFM	0 – 3, lower to higher	Cellularity	0 – 3, fewer - more
IFM width	0 – 3, smaller to larger	Nucleus shape	0 – 3, elongated to rounded
Cellularity	0 – 3, fewer - more	Organisation of collagen fibres	0 – 3, linear to non-linear
		Crimp angle	0 – 3, smaller to larger

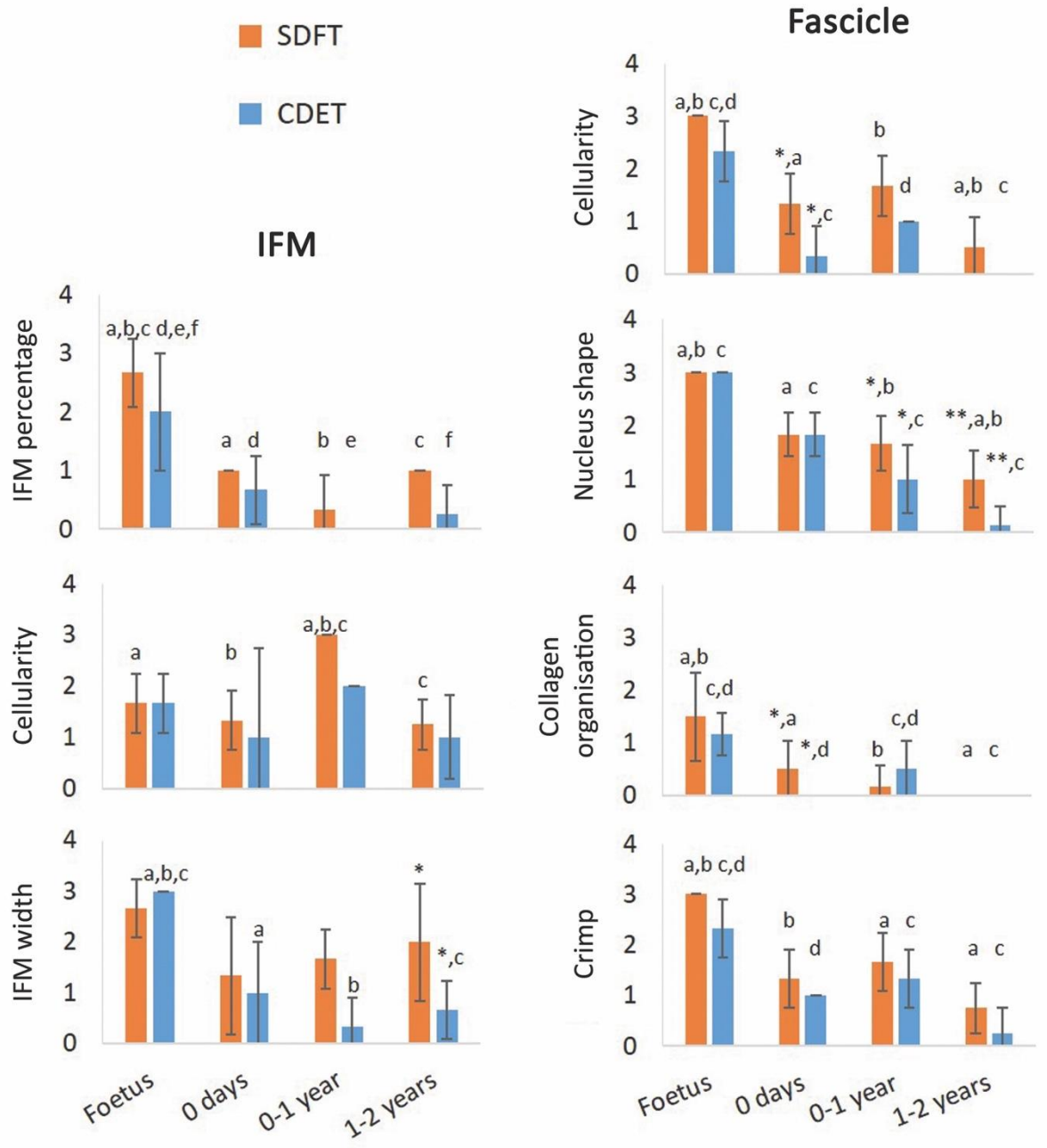

Figure 3 – Figure supplement 1. Scoring of histologic variables for the IFM and fascicle in the SDFT and CDET through postnatal development. * significant difference between tendons, a-f significant difference between age groups. Error bars depict standard deviation.

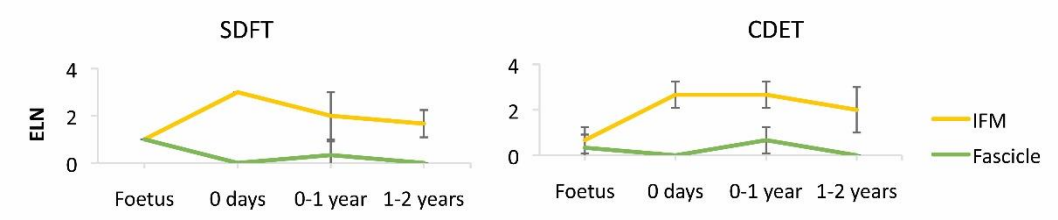

Figure 4 – Figure supplement 1. Scoring of ELN staining for the IFM and fascicle in the SDFT and CDET through postnatal development. Error bars depict standard deviation.

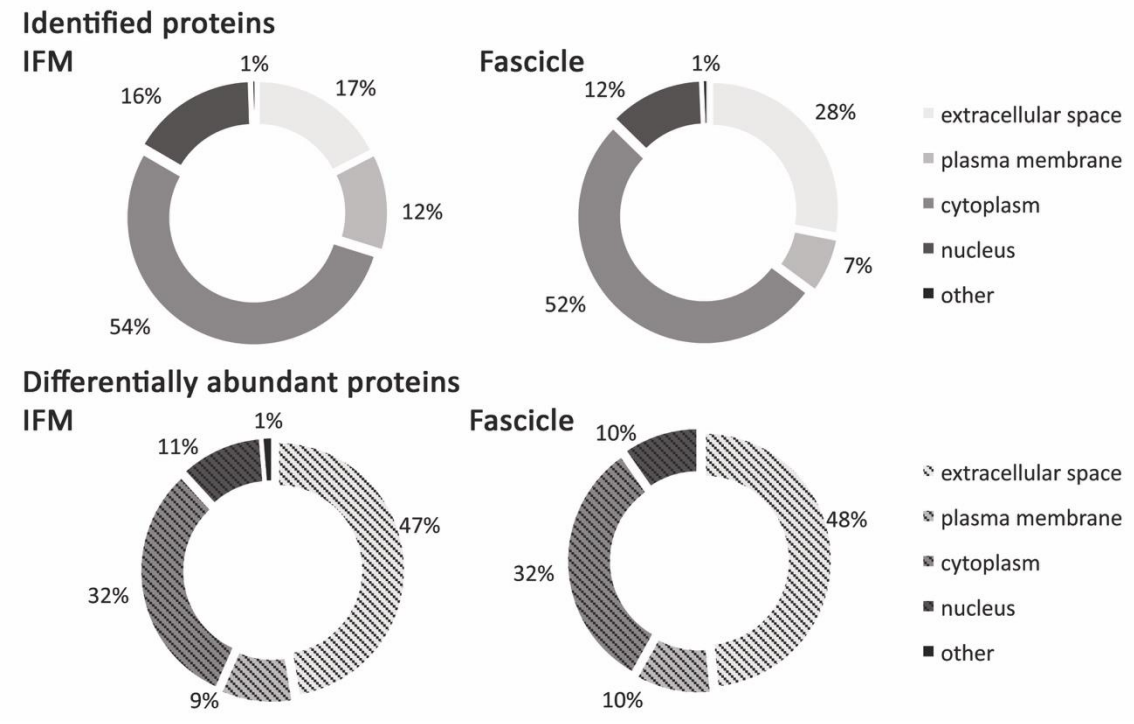

Figure 5 – Figure supplement 1. Classification of SDFT IFM and fascicle identified proteins and differentially abundant proteins (p<0.05, fold change≥2) according to their associated location.

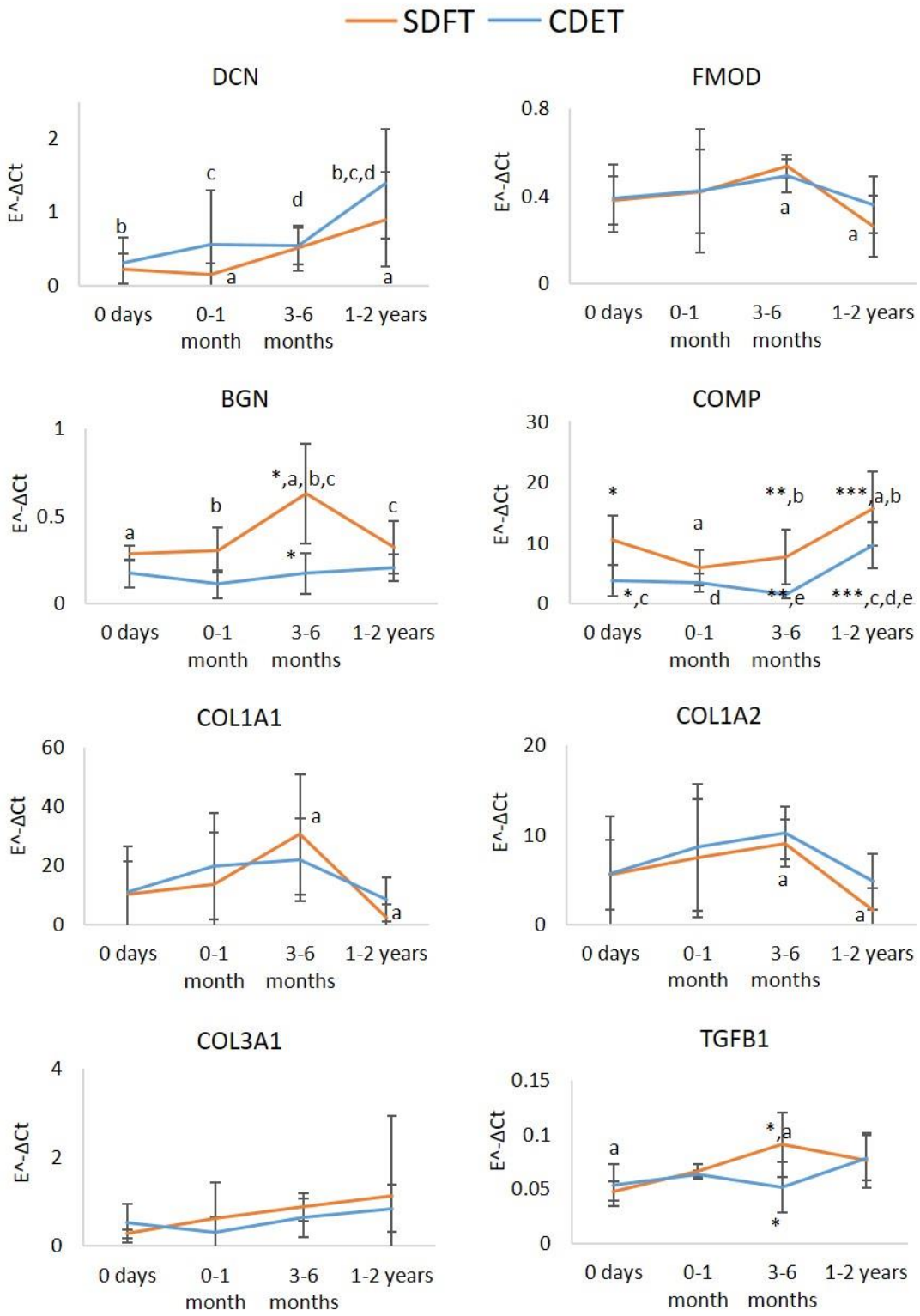

964

965 **Figure 5 – Figure supplement 2. Relative mRNA expression of major ECM genes in**

966 **whole tissue SDFT and CDET through postnatal development.** * significant difference

967 between tendons, a-e significant difference between age groups. Error bars depict standard

968 deviation.